THE ASTROPHYSICAL JOURNAL, 400:435–459, 1992 December 1

SEARCH FOR PARTIAL SYSTEMIC LYMAN EDGES IN NEARBY QUASARS

A. P. KORATKAR, A. L. KINNEY, AND R. C. BOHLIN
Space Telescope Science Institute, 3700 San Martin Drive, Baltimore, MD 21218
Received 1992 January 27; accepted 1992 June 6

ABSTRACT

The Lyman edge region (912 Å) of quasars is thought to be formed by thermally emitting accretion disks and would be affected by broad-line region (BLR) clouds. The Lyman edge discontinuities in disk models are predicted both in absorption ($\lesssim 80\%$) and in emission ($\lesssim 30\%$). For BLR clouds, the predictions range from complete absorption at the Lyman edge for large BLR clouds to ubiquitous ($\sim 10\%$) absorption edges for an isotropic mist of clouds. The *IUE* archives provide a number of objects to search for the features predicted by these different models. By optimally extracting spectra and co-adding multiple spectra, a systematic search for discontinuities as small as 15% is possible in the typical S/N spectra.

In our sample of 49 quasars, 38% of the AGNs do not show any discontinuity at any redshift. Discontinuities at redshifts smaller than the AGN emission redshift are seen in 28% of the sample. These discontinuities are associated with intervening gas extrinsic to the AGN environment. Discontinuities at the AGN emission redshift potentially due to associated gas in the AGN environment are seen in 22% of the sample. However, only 10% of the sample shows discontinuities at the emission redshift which cannot be associated with any known absorption-line systems.

Our analysis indicates that only those accretion disk models in which most of the AGNs show Lyman edge discontinuities of $\lesssim 15\%$ are consistent with the observations. If the Lyman edge discontinuity is due to large BLR clouds, the observations indicate that the gas column densities are less than $\approx 10^{22}$ cm^{-2}.

Subject headings: galaxies: active — quasars: absorption lines

1. INTRODUCTION

A detailed analysis of the continuous spectral region near the Lyman edge (912 Å) is important, because the shape of the continuum in this region is a powerful diagnostic of the emission mechanism of the UV flux in active galactic nuclei (AGNs). Any excess Lyman continuum absorption at the quasar redshift is also evidence of absorbing material in the line of sight intrinsic to the quasar or its environment. We have searched *IUE* archival spectra of quasars with redshifts $0.4 \leq z \leq 2.3$ for changes in the continuum at the systemic Lyman edge positions. The results of the analysis provide constraints on the current models.

The mechanism that powers quasar activity is believed to be gravitational energy released during accretion of gas onto a supermassive (10^7–10^9 $M_\odot$) blackhole (Salpeter 1964; Zel'dovich & Novikov 1964; Lynden-Bell 1969). Removal of angular momentum and a certain amount of gravitational energy from the accretion flow leads to the formation of an accretion disk (see the review by Begelman 1985 for details). Hence, existence of an accretion disk in AGN is an attractive theoretical idea, but definitive observational evidence does not exist. One of the observational facts that favors the disk models is the *big blue bump* component of the quasar continuum, which extends from 1 μm to the soft X-ray region. This feature may be due to thermal emission from the surface of an accretion disk at temperatures in a range centered at 30,000 K (Shields 1978; Malkan 1983). The accretion disk models not only interpret the big blue bump, but also make predictions about the emission-line profiles (Collin-Souffrin & Dumont 1990; Eracleous & Halpren 1992a, b), polarization (Antonucci 1987; Laor, Netzer, & Piran 1990; Antonucci 1992), and the discontinuity at the Lyman edge (Kolykhalov & Sunyaev 1984; Sun & Malkan 1989a, b; Laor & Netzer 1989; Netzer 1992; Czerny & Pojmanski 1990; Czerny & Zbyszewska 1991).

The Lyman continuum in quasars can be affected in another way. The energy released by the central source can be absorbed by the broad-line region (BLR) gas surrounding the power source. Thus, models predict absorption shortward of 912 Å in at least a few lines of sight. The form of the absorption depends on the fraction ($\omega/4\pi$) of the central power source covered by the BLR clouds, the size of these clouds, and the overall geometry and kinematics of the region.

A study of this wavelength region provides constraints for models that attempt to explain the big blue bump and could also provide a direct measure of the BLR gas covering factor. This study presents observations of the discontinuity at the Lyman edge (912 Å) for moderate redshift AGNs. The nature of the Lyman continuum is compared with predictions made by (1) optically thick, geometrically thin accretion disk models and (2) BLR cloud models (Carswell & Ferland 1988).

Observational results of spectroscopic investigations near the Lyman edge are reported in the literature as follows. Smith et al. (1981) found partial or total Lyman discontinuity near the intrinsic redshift in 14 out of 32 high redshift quasars. Baldwin & Smith (1983) studied eight of these 14 quasars and concluded that the Lyman discontinuity was *not* intrinsic to the quasar based on the nature of the associated narrow Lyα absorption line. MacAlpine & Feldman (1982) studied 17 high redshift quasars and found no definite Lyman discontinuity. The recent investigation for the Lyman discontinuity in 11 high-redshift quasars by Antonucci, Kinney, & Ford (1989) found only two quasars with partial edges. Their observations of the Lyα λ1216 emission line showed that the edge in these two objects cannot conclusively be associated with an accretion disk. Investigations by Kinney et al. (1991a) of intermediate- and high-redshift quasars observed by the *IUE* showed that five of the 28 objects investigated had Lyman discontinuities within the velocity width of the broad emission

TABLE 1

LIST OF OBJECTS

Object Name (1)	Mag (V) (2)	z (3)	$E(B-V)$ (4)	Number of Spectra (5)	Data Quality (6)	D (%) (7)	S(D) (8)	Lyman Edge (9)	Comment (10)
0002+051	16.21	1.899	0.026	LW 1	Q3	6	2	$z_{abs} < z_{em}$	Radio
0003+158	16.40	0.450	0.024	SW 1	Q1	−8	2	No edge	Radio
0043+008	17.00	2.143	0.002	LW 1	Noise	...	...	...	Radio
0044+030	16.00	0.624	0.018	SW 1	Noise	...	...	...	
0105+061	17.20	1.960	0.016	LW 1	Noise	...	...	...	
0117+213	16.05	1.493	0.036	LW 1	Q2	95	12	Candidate	
0133+004	18.50	0.910	0.003	SW 1	Noise	...	...	...	
0215+015	18.33	1.715	0.022	LW 8	Q2	73	40	$z_{abs} \approx z_{em}$	Blazar
0219+428	15.50	0.444	0.098	SW 5	Q3	9	5	No edge	Blazar, artifact
0232−042	16.46	1.436	0.004	LW 2	Noise	...	...	...	Radio
0237−233	16.63	2.223	0.007	LW 1	Q3	4	1	$z_{abs} < z_{em}$	Radio
0302−223	16.00	1.400	0.005	LW 1	Q3	100	17	$z_{abs} \approx z_{em}$	
0405−123	14.82	0.574	0.018	SW 7	Q1	23	101	Candidate	Radio
0414−060	15.94	0.781	0.030	SW 2	Q3	19	13	No edge	Radio, artifact
0454−220	16.10	0.534	0.006	SW 1	Q2	100	58	$z_{abs} \approx z_{em}$	Radio
0454+039	16.53	1.345	0.058	LW 2	Q3	...	4	No edge	Radio
0537−441	15.50	0.894	0.020	SW 1	Q3	...	...[a]	...	Blazar
0637−752	15.75	0.656	0.111	SW 2	Q1	0	1	No edge	Blazar
0735+178	14.85	0.424	0.090	SW 6	Q1	100	88	$z_{abs} \approx z_{em}$	Blazar
0742+318	16.00	0.462	0.039	SW 2	Q3	10	2	No edge	Radio
0743−673	16.37	1.512	0.173	LW 1	Q2	10	4	Candidate	Radio
0932+501	17.24	1.920	0.007	LW 1	Noise	...	...	...	
0935+417	16.25	1.980	0.004	LW 1	Q3	−18	3[a]	$z_{abs} < z_{em}$	
0955+326	15.78	0.533	0.014	SW 5	Q3	...	...	...[a]	Radio, artifact
0957+561	17.00	1.405	0.000	LW 12	Q2	95	21	$z_{abs} \approx z_{em}$	Radio
0958+550	16.00	1.758	0.005	LW 1	Q3	103	13	$z_{abs} \approx z_{em}$	
1007+417	16.50	0.611	0.000	SW 1	Q2	−8	3	No edge	Radio
1011+250	15.40	1.631	0.026	LW 3	Q2	101	35	$z_{abs} \approx z_{em}$	Radio
1101−264	16.02	2.145	0.049	LW 1	Q3	13	4	$z_{abs} < z_{em}$	Blazar
1103−006	16.46	0.426	0.021	SW 1	Q3	43	5	No edge	Radio
1136−135	16.08	0.557	0.010	SW 1	Q3	...	...[a]	...	Radio, artifact
1137+660	16.32	0.646	0.001	SW 1	Q1	11	5	No edge	Radio
1138+040	16.05	1.876	0.000	LW 1	Noise	...	...	...	
1148+549	15.82	0.969	0.000	SW 3	Q3	11	7	No edge	Artifact
1156+295	14.41	0.729	0.000	SW 4	Q3	0	0	No edge	Blazar, artifact
1206+459	15.79	1.158	0.016	SW 2	Noise	...	...	...	
1215+113	16.86	1.396	0.004	LW 1	Noise	...	...	...	Radio
1225+317	15.87	2.219	0.008	LW 3	Q2	17	5	$z_{abs} < z_{em}$	Radio
1241+176	15.38	1.273	0.011	LW 6	Q2	...	...[a]	...	
1246−057	16.73	2.236	0.009	LW 1	Noise	...	...	...	
1247+267	15.80	2.038	0.005	LW 1	Q3	29	9[a]	$z_{abs} < z_{em}$	
1248+401	16.06	1.030	0.000	SW 1	Q2	−23	7	$z_{abs} < z_{em}$	
1253−055	17.75	0.538	0.013	SW 4	Q3	6	4	No edge	Blazar, artifact
1257+346	16.79	1.375	0.001	LW 1	Noise	...	...	...	Radio
1259+593	15.60	0.472	0.000	SW 1	Q3	19	6	No edge	Artifact
1303+308	17.85	1.759	0.000	LW 1	Noise	...	...	...	
1309−056	17.44	2.224	0.016	LW 1	Noise	...	...	...	
1317+277	15.98	1.022	0.024	SW 2	Q2	−11	4	$z_{abs} < z_{em}$	
1318+290	16.90	0.549	0.000	LW 1	Noise	...	...	...	
1327−206	17.04	1.169	0.058	LW 1	Noise	...	...	...	Radio
1329+413	16.30	1.930	0.000	LW 2	Noise	...	...	...	
1331+170	16.71	2.081	0.000	LW 2	Q2	97	20	$z_{abs} < z_{em}$	Radio
1333+176	15.64	0.554	0.004	SW 1	Noise	...	...	...	
1338+416	16.08	1.219	0.000	LW 1	Q3	44	22	Candidate	
1352+011	16.03	1.121	0.013	SW 1	Noise	...	...	...	
1354+195	16.02	0.720	0.013	SW 1	Q2	−3	1	$z_{abs} < z_{em}$	Radio
1407+265	15.73	0.944	0.000	SW 2	Q1	1	1	No edge	
1421+331	16.70	1.904	0.000	LW 1	Q3	1	2	$z_{abs} < z_{em}$	
1435+638	15.00	2.060	0.011	LW 1	Noise	...	...	...	Radio
1522+102	15.74	1.321	0.020	LW 1	Q3	42	29[a]	$z_{abs} < z_{em}$	Artifact
1526+285	16.40	0.450	0.010	SW 1	Noise	...	...	...	
1538+447	16.01	0.770	0.007	SW 2	Q3	99	44	Candidate	
1630+377	15.96	1.471	0.000	LW 1	Q2	−19	10[a]	No edge	
1634+706	14.90	1.334	0.057	LW 13	Q2	18	15	$z_{abs} < z_{em}$	
1641+399	15.96	0.595	0.000	SW 4	Q3	52	26	$z_{abs} \approx z_{em}$	Blazar, artifact
1715+535	16.30	1.920	0.014	LW 1	Q3	−15	2	No edge	
1718+481	15.33	1.084	0.020	SW 2	Q1	3	3	$z_{abs} < z_{em}$	
1912−550	16.49	0.402	0.047	SW 1	Q2	125	8	$z_{abs} \approx z_{em}$	Radio
2112+059	15.52	0.466	0.067	SW 1	Noise	...	...	...	

TABLE 1—*Continued*

Object Name (1)	Mag (V) (2)	z (3)	E(B−V) (4)	Number of Spectra (5)	Data Quality (6)	D (%) (7)	S(D) (8)	Lyman Edge (9)	Comment (10)
2128−123.....	15.46	0.501	0.041	SW 3	Q2	89	36	$z_{abs} \approx z_{em}$	Radio
2216−038.....	16.52	0.901	0.049	SW 1	Noise	...	...	...	Radio
2223−052.....	17.19	1.404	0.048	LW 9	Noise	...	...	...	Blazar
2237+031.....	16.78	1.695	0.036	LW 1	Noise	...	...	...	
2251+158.....	16.10	0.859	0.064	SW 1	Noise	...	...	...	Blazar
2302+029.....	16.03	1.044	0.057	SW 1	Q3	24	11[a]	No edge	
2308+098.....	16.00	0.432	0.022	SW 3	Q3	63	32[a]	No edge	Radio, artifact
2326−477.....	16.79	1.299	0.000	LW 1	Q3	108	10	$z_{abs} \approx z_{em}$	Radio
2344+092.....	15.97	0.672	0.041	SW 1	Q2	33	7	No edge	Radio

[a] See Appendix A.

lines. However, these objects had associated narrow absorption lines in Lyα λ1216, C IV λ1549, and Mg II λ2798; and the discontinuity could be attributed to an intervening absorber like the BLR clouds or the host galaxy. Four of the 28 objects showed discontinuities at redshifts less than the quasar redshift. The investigations by Kinney et al. concluded that there were no detectable intrinsic Lyman discontinuities which could be unambiguously associated with accretion disks.

2. DATA REDUCTION AND ANALYSIS

An investigation of the kind proposed here has only been conducted with high signal-to-noise (S/N) spectra for a few high-redshift objects (Antonucci et al. 1989). Here we study quasars with redshifts in the range 0.4–2.40 and with spectra available in the *IUE* archives. With optimal extraction (Kinner, Bohlin, & Neill 1991b) and co-addition the S/N of *IUE* spectra in this sample ranges between 20 to 3 per 75 Å. Since the fitting procedure used in the analysis includes 75–225 data points, the effective S/N is improved, and partial discontinuities as small as 15% can be detected for a typical spectrum.

Table 1 is a list of all objects with redshifts between 0.4 and 2.4 in the *IUE* archives. The *V* magnitudes and redshifts in the table are taken from Hewitt & Burbidge (1987). The radio-loud designations, indicated by the word "Radio" in column (10), are based on Veron-Cetty & Veron (1987). In the same column, the classical BL Lacertae objects, optically violent variables, and high polarization quasars are denoted as "Blazars." The blazars are from the lists of Angel & Stockman (1980) and Moore & Stockman (1981). Since the UV spectral shapes can be affected by Galactic reddening, the spectra are corrected for Galactic reddening using the $E(B-V)$ values in Table 1 from Burstein & Heiles (1984). The *IUE* camera and the number of spectra per object are also given. There are 78 quasars, 39 of which have their intrinsic Lyman edge region in the short-wavelength camera (SWP) and 39 of which have their Lyman edge region in the long wavelength (LWP or LWR) camera.

Of the 78 objects, 28 have more than two spectra, which are co-added to improve the S/N. For objects with multiple spectra, the spectra were normalized to that spectrum with the median flux value. Although some quasars showed appreciable variability in the UV, no wavelength-dependent variability was seen in the Lyman edge feature. In those cases when the Lyman edge falls close to the cutoff between SW and LW cameras, variability can be problematical. These cases are discussed in the Appendix A. To determine the quality of the spectra, the following procedure is used. First, the average level of the percent noise (100N/S) in a region 250 Å wide on the short-wavelength (N_1) and long-wavelength (N_2) sides of the Lyman edge is determined. Next, a "weighted noise" is determined, as defined by $N_w = (N_1^2/n_1 + N_2^2/n_2)^{1/2}$, where N_1 and N_2 are the average noise levels, and n_1 and n_2 are the number of data points in the regions on either side of the Lyman edge. If both $N_1, N_2 \geq 60\%$, and $N_w > 7.5\%$, the spectra are considered noisy and deleted from further analysis. In some spectra, the highly nonstatistical nature of the *IUE* noise did not allow the fitting routine to converge. These spectra are also deleted from the analysis. There are 25 objects, indicated in Table 1 with "Noise" in column (6), which have noisy data or highly nonstatistical noise in the spectra. If both N_1, $N_2 \leq 20\%$, and $N_w < 5\%$, then the spectra are denoted in Table 1 as quality 1 (Q1). If $N_1 \leq 20\%$ and $N_2 > 20\%$, then the spectra are denoted as quality 2 (Q2). If both N_1 and $N_2 > 20\%$ then the spectra are denoted as quality 3 (Q3). *IUE* artifacts (see next paragraph) are prominent in some spectra. These are denoted in Table 1 by the word "Artifact" in column (10) and have been assigned data quality 3. There are 53 AGNs in the analysis of which 24 are radio-loud AGNs and nine are blazars. Figure 1 shows examples of spectra with qualities 1, 2, and 3.

The reextracted spectra are analyzed as follows. A power law of the form

$$f_\lambda = b_1 \lambda^{b_2} + b_3 \quad (1)$$

is fitted to the continuum for wavelengths below the observed position of 912 Å. The continuum for wavelengths longer than 912 Å included the Lyβ/O VI λ1034; and, hence, the fitting function has the form

$$f_\lambda = b_4 \lambda^{b_5} + b_6 + b_7 e^{(\lambda - b_8)^2/2b_9^2}, \quad (2)$$

where $b_1, b_2, b_3, \ldots, b_9$ are the fitted parameters. The best fit is achieved by minimizing the χ^2. Two independent power laws are fitted over a 250 Å region on either side of the Lyman edge, excluding a region $\approx$30 Å ($\pm$ 10,000 km s^{-1}) at the edge. This exclusion is to accommodate the theoretical velocity broadening and possible curvature in the continuum (predicted by accretion disk models or due to blending of Lyman absorption lines) which cannot be handled by power-law fits. Further, a large wavelength region was investigated because the Lyman edge could be shifted in wavelength depending on the geometry of the material causing the edge (see § 4.2 for references). In two objects (1338+416 and 1538+477) the 30 Å gap had to be widened to accommodate the strong curved continuum. The fitting procedure excludes the geocoronal Lyα λ1216 region and the *IUE* camera artifacts discussed by Crenshaw, Bruegman, & Norman (1990). The regions excluded are

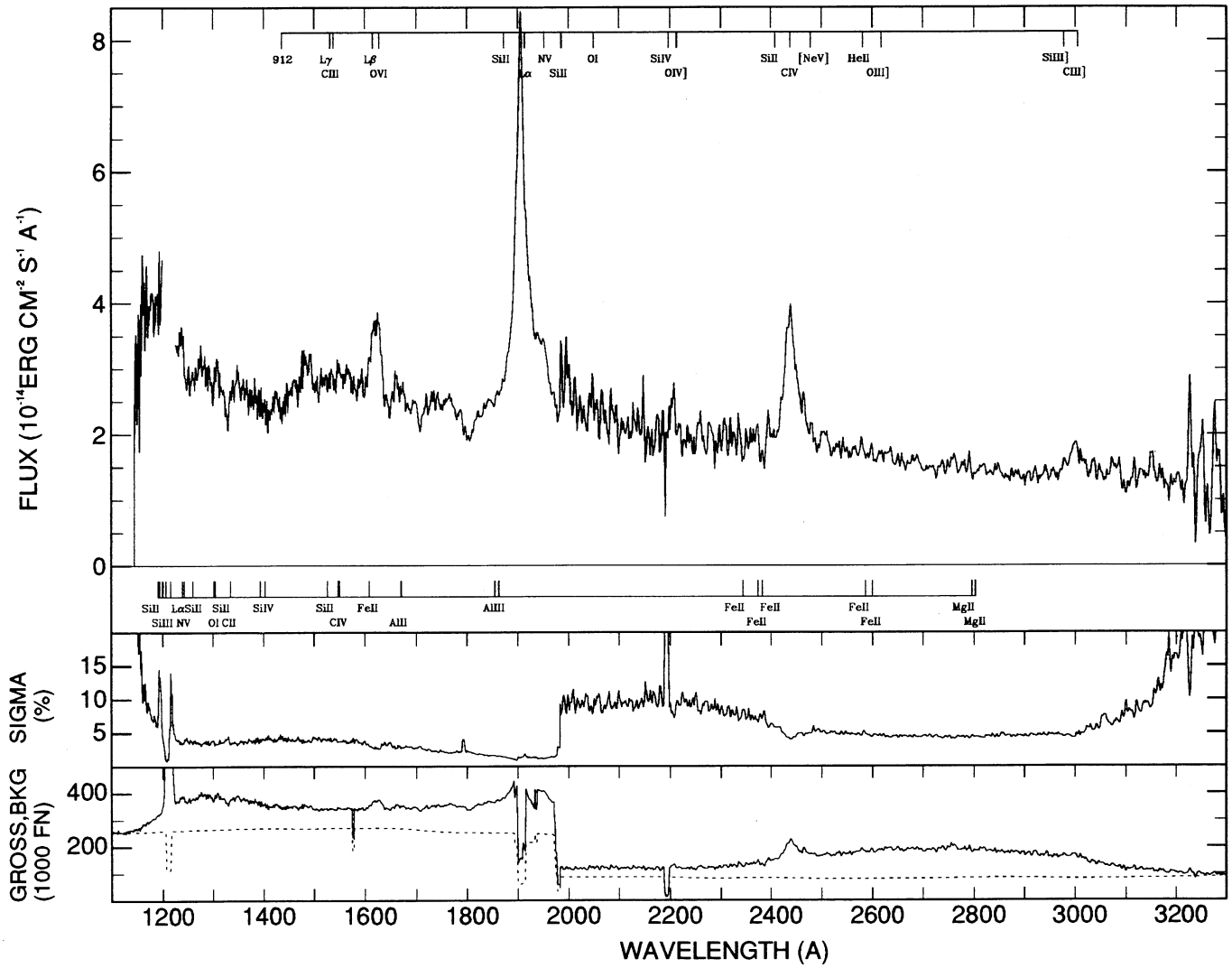

FIG. 1*a*

FIG. 1.—Optimally extracted sample spectra where (*a*) is quality 1, for 0405−123; (*b*) is quality 2, for 1007+417; and (*c*) is quality 3, for 1247+267. The gross FN is shown at the bottom of each plot as a solid line; the background is a dotted line. Above the gross and background FN, the noise is plotted as a percentage of the total flux. The spectrum itself is plotted in units of ergs cm^{-2} s^{-1} $Å^{-1}$. A horizontal bar is drawn at the top of the plot, with the location of typical emission lines marked at the redshift of the quasar.

(1200–1230), 1277–1281), (1286–1290), and (1660–1666) in the SWP spectra. Since the artifacts in the LWP and LWR cameras are of low contrast, no spectral regions are excluded in the 2000–3200 Å LW spectra. Any complex absorption features due to the Lyman forest, are ignored in the fitting procedure. An apparent emission-like feature is sometimes observed just above the observed Lyman edge. There is no strong UV emission line corresponding to that position (Sofia, Bruhweiler, & Kafatos 1989). This feature is in some cases due to the broad complex artifact at 1500 Å (see Crenshaw et al. 1990). In some other cases the Lyman absorption features are strong and together with the Lyman edge make the region seem to have spurious emission-line features. Where such a feature seems prominent, we have noted this for each individual case in Appendix A.

The fits for the analysis are shown in Figure 2 for all objects not deemed noisy in Table 1. For objects with Lyman limit absorption at redshifts much less than the AGN emission redshift ($z_{abs} < z_{em}$), fits to both the regions around z_{em} and z_{abs} are shown as two separate plots. The position at which the systemic Lyman edge is expected is marked in the first plot, and the position of the Lyman edge corresponding to the z_{abs} is marked in the additional plot. For objects with no discontinuity, only the power-law fit (eq. [1]) to the region around the Lyman limit is shown. The position at which the systemic Lyman edge is expected is marked. The significance of the Lyman edge discontinuities in four objects (0537−441, 0955+326, 1136−135, 1241+176) is low (see Appendix A for details). These objects have been shown in Figure 3 and have been removed from further analysis.

The reality of the Lyman edge discontinuities was established as follows. The wavelength range on both sides of the Lyman edge was fitted by a single power law. This power law fit was compared with the fits on either side of the Lyman edge described above. If the reduced χ^2 of the single power law was smaller than the reduced χ^2 of the fits on either side 912 Å, the

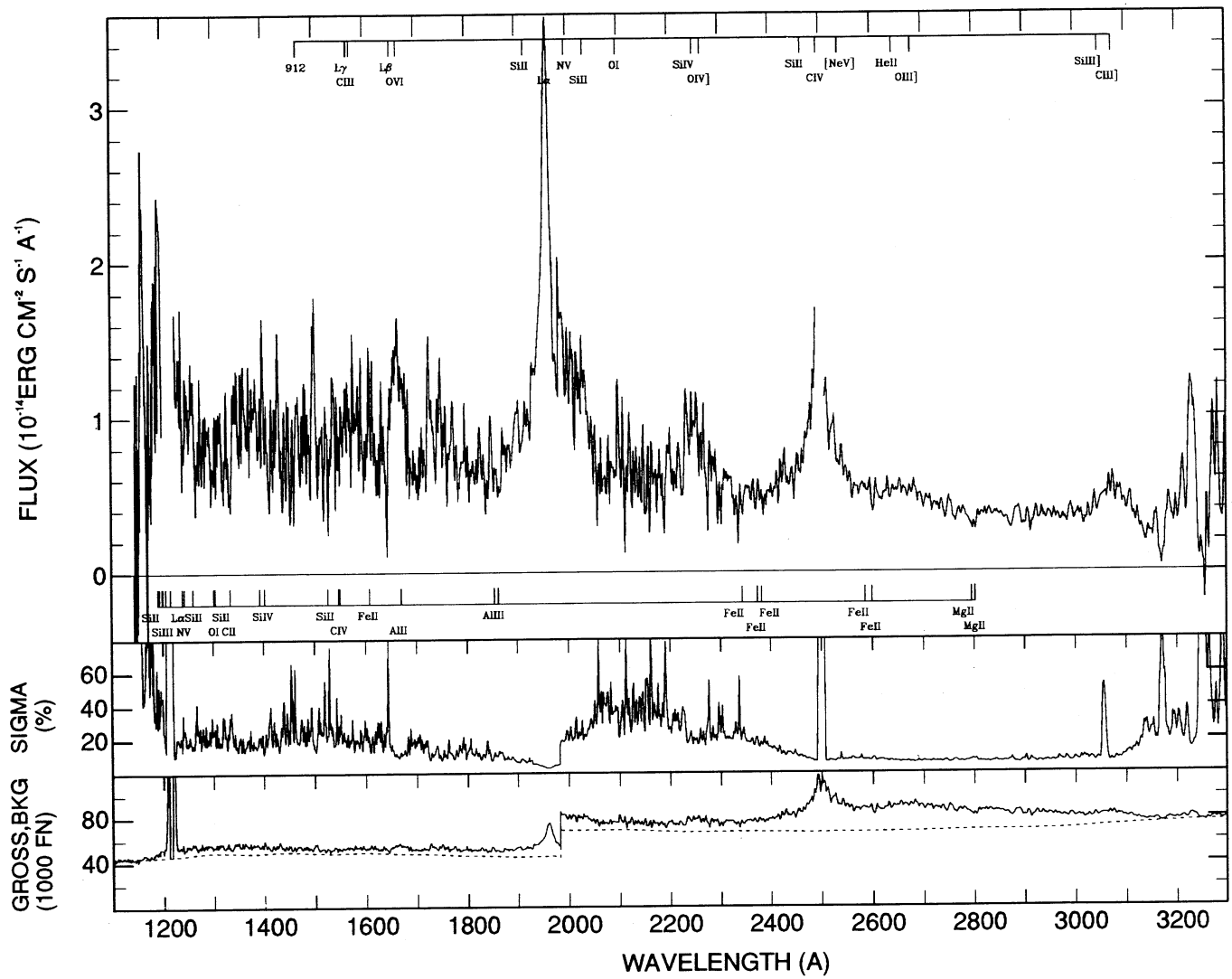

FIG. 1*b*

region was considered to show no Lyman edge discontinuity. The percentage discontinuity ($D\% = 100(F_+ - F_-)/F_+$, where F_+ is the flux at 912^+ and F_- is the flux at 912^-) is calculated and given in Table 1. The significance of the discontinuity, $S(D) = D/(\sigma/n)^{1/2}$, where D is the amount of discontinuity, σ is the 1 σ variation in the flux, and n is the total number of points in the fit, is calculated. $S(D)$ is also given in Table 1. AGNs with no Lyman edge discontinuity in the *IUE* wavelength range and no significant change in the power-law slopes across the Lyman edge are indicated in Table 1 as "No Edge" in column (9). AGNs with discontinuities at redshifts much less than the AGN emission redshift are indicated in Table 1 by "$z_{abs} < z_{em}$." AGNs with discontinuities at the quasar redshift and associated metal absorption lines are shown in Table 1 as "$z_{abs} \approx z_{em}$." AGNs with discontinuities at the quasar redshift and no associated metal absorption lines are shown in Table 1 as "candidate." There are no edges detected in emission. Individual objects are discussed in detail in the Appendix A.

O'Brien et al. (1988) used the *IUE* archives to investigate the shape of the Lyman continuum. There are 17 objects from that study in common with the present data set. For seven of the objects the continuum slopes below Lyα are consistent with our measurements ($\Delta\alpha = 0.06$). For the remaining 10 objects the $\Delta\alpha = 0.19$. We attribute this difference to the presence of artifacts, and the small Lyman edge discontinuities which affect the fitting procedure. We confirm the observation by O'Brien et al. that the slope of the Lyman continuum is a function of redshift. This is because most objects at lower redshifts do not show Lyman edges, while objects with higher redshifts show Lyman absorption edges.

3. RESULTS

The 49 AGNs can be separated into four groups according to the nature of their Lyman edges. The results of this grouping are summarized in Table 2, which shows that there is no preference for the radio-loud or radio-quiet objects in any one of the groups. The particulars of each group are discussed below.

3.1. *Group 1: No Discontinuities in Entire IUE Range*

These are 19 AGNs which form 39% of the sample. The sensitivity limit of our data set is $\approx 15\%$ for the Lyman discontinuities.

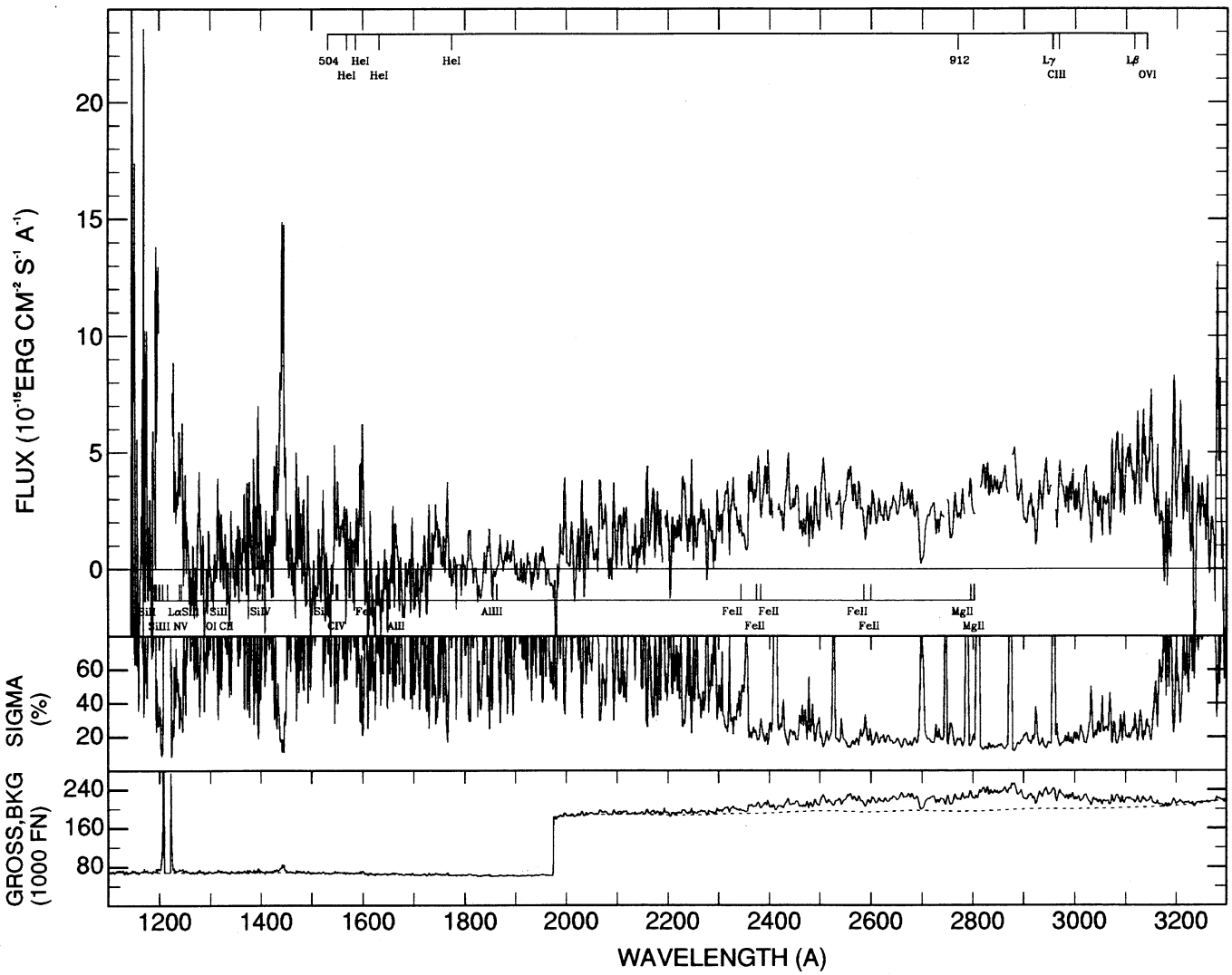

FIG. 1c

3.2. *Group 2: Discontinuities at* $z_{abs} < z_{em}$

This group contains all objects which show Lyman edges in the *IUE* range and have an absorption edge which is more than 20,000 km s^{-1} from the expected intrinsic Lyman edge of the quasar. This group forms 29% of the sample and is listed in Table 3. Shown in column (2) are the percentage discontinuities; column (3), the significance of these discontinuities; column (4), the redshifts at which the Lyman edge is found; column (5), the velocity of the Lyman absorption relative to the quasar emission redshift (v/c); column (6), any metal absorption line found in the literature corresponding to the Lyman edge; column (7), the redshift of the line; column (8), the reference for the absorption-line observation; and column (9), any other references to absorption in that quasar found in the literature. Any redshift discrepancy between the Lyman edge and the corresponding absorption lines is presumably either due to measuring error (≈ 8 Å) or due to blending of high n Lyman absorption lines. 0215+015 shows absorption both at z_{em} as

TABLE 2

SUMMARY OF RESULTS

Group Type	Total Number	Number of Radio-loud Objects	Number of Blazars	Percentage of Sample (%)	Narrow-Line Absorption
No discontinuity	19	9	4	39	...
$z_{abs} < z_{em}$	14	5	1	29	Yes
$z_{abs} \approx z_{em}$	11	6	2	22	Yes
$z_{abs} \approx z_{em}$	5	2	1	10	No

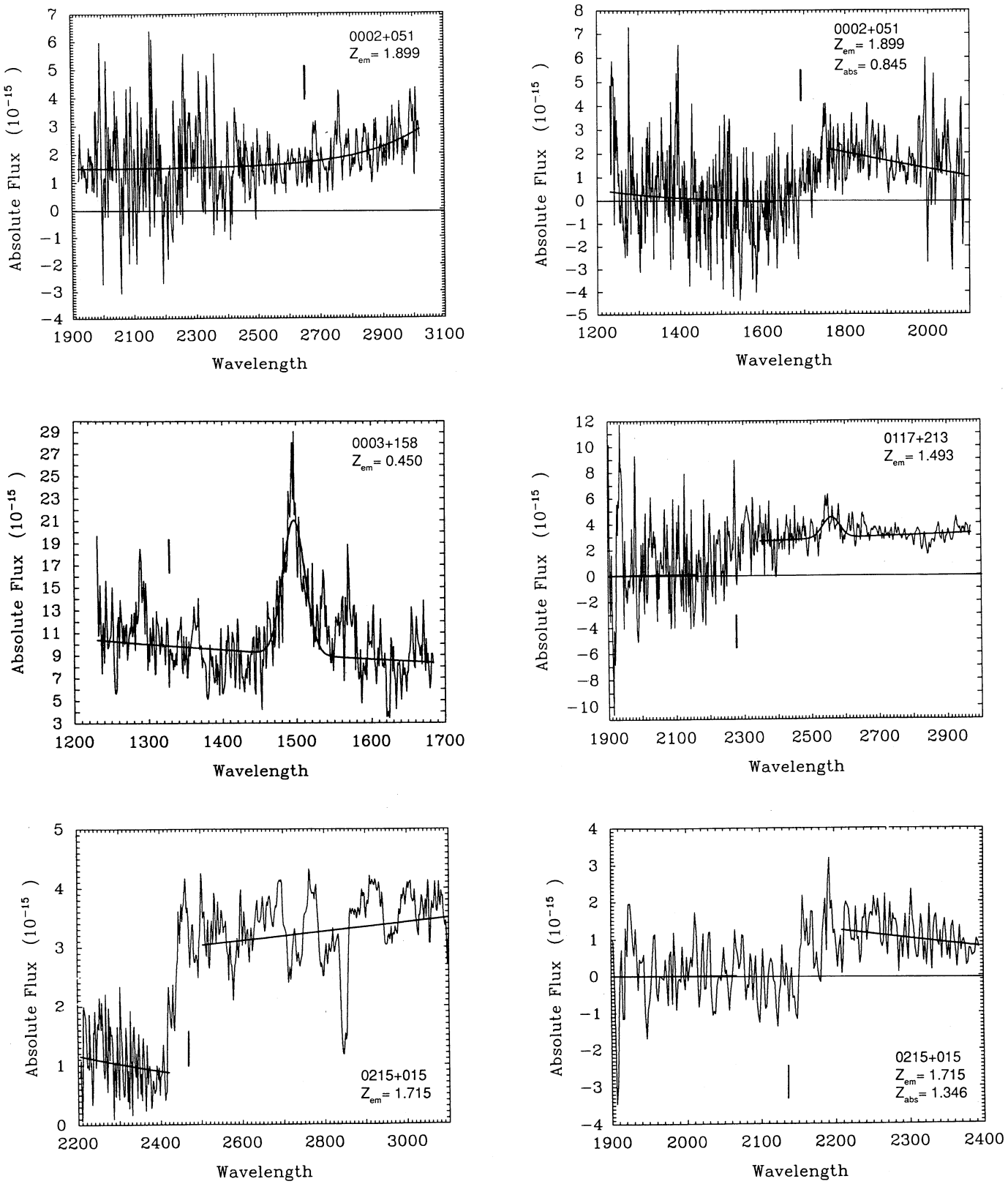

FIG. 2.—Continuum power-law fits to the objects in the analysis (excluding those indicated as noise in Table 1), according to eqs. (1) and (2). The units of flux are ergs cm^{-2} s^{-1} $Å^{-1}$, and the observed wavelength is in angstroms. Objects which show no Lyman edges are fitted by single power law across the Lyman edge at z_{em}. The position at which the systemic Lyman edge is expected is marked. For objects with Lyman edges at redshifts smaller than the quasar emission redshifts ($z_{abs} < z_{em}$), an additional plot of the region around 912 Å for z_{abs} is shown. The position at which the systemic Lyman edge is expected is marked in the first plot and the position of the Lyman edge corresponding to the z_{abs} is marked in the additional plot.

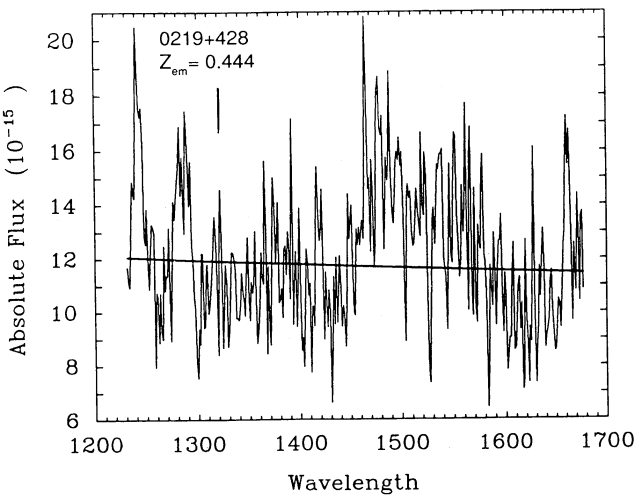

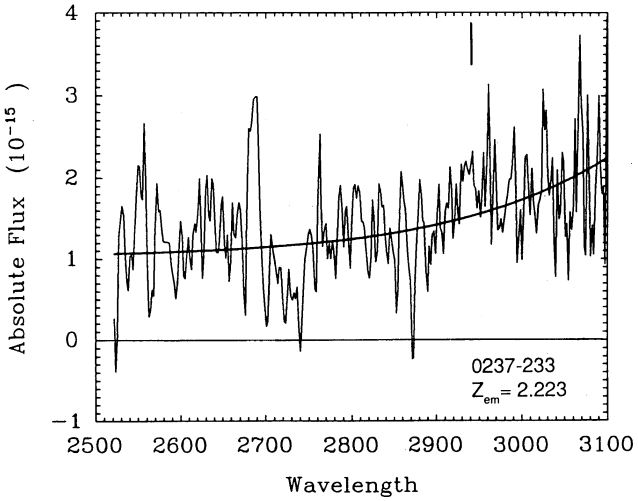

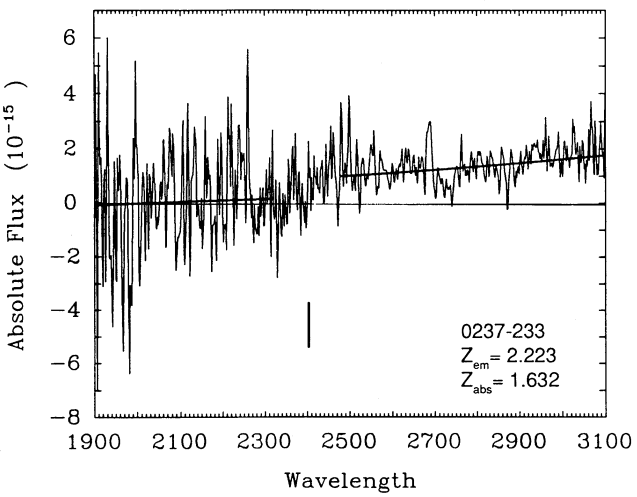

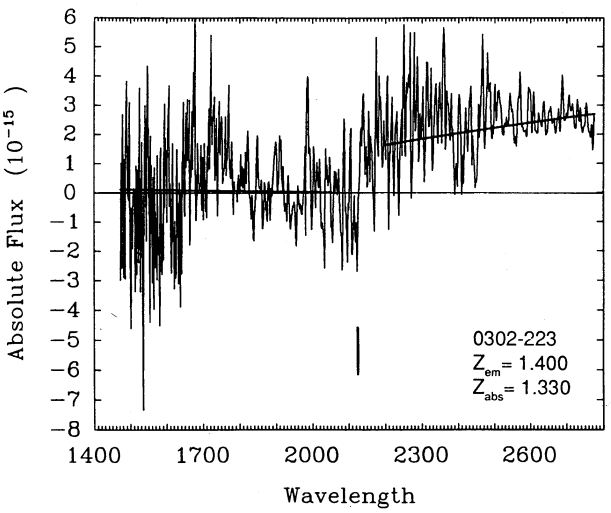

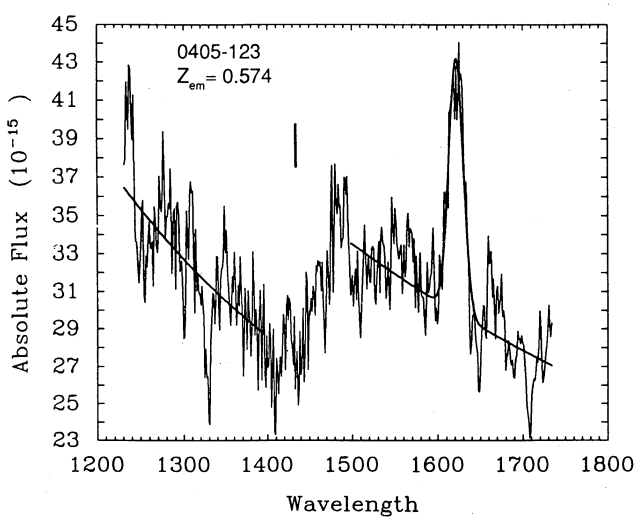

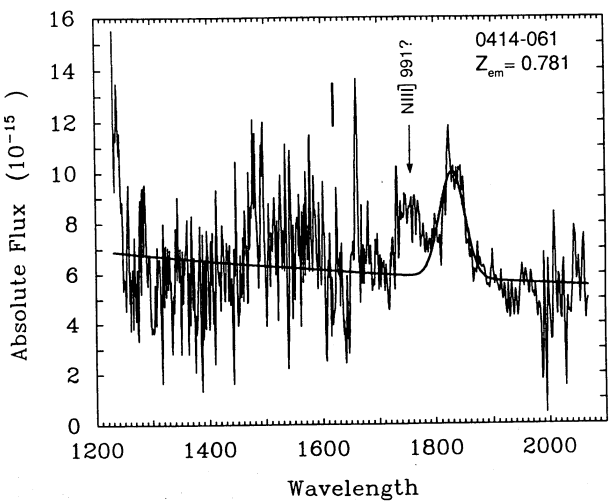

FIG. 2—*Continued*

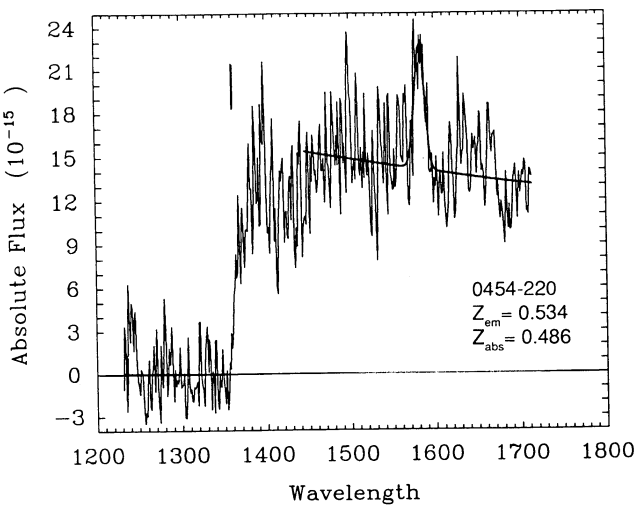

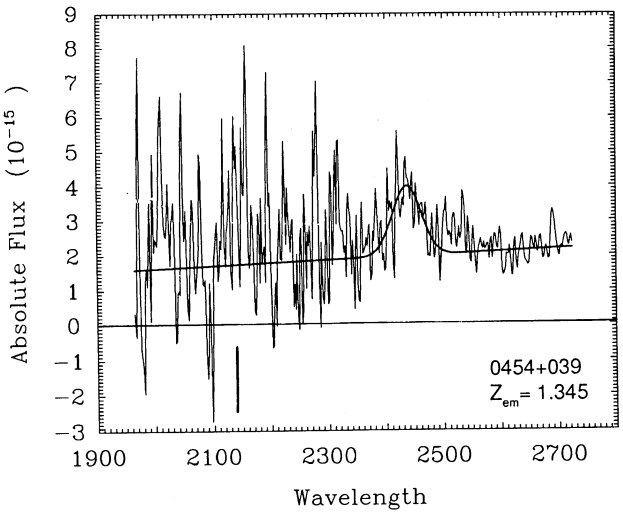

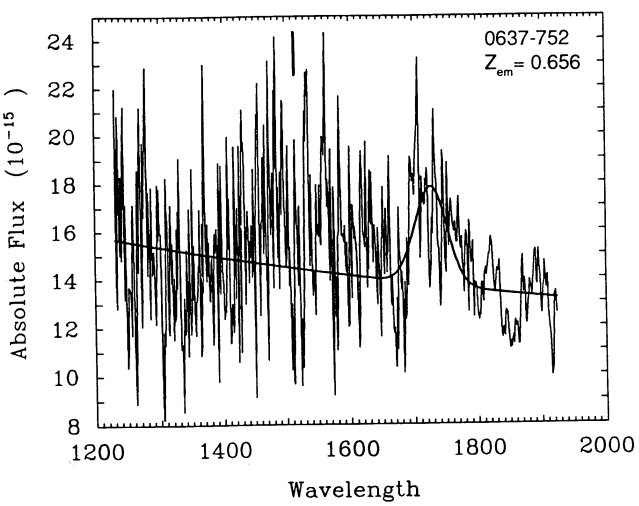

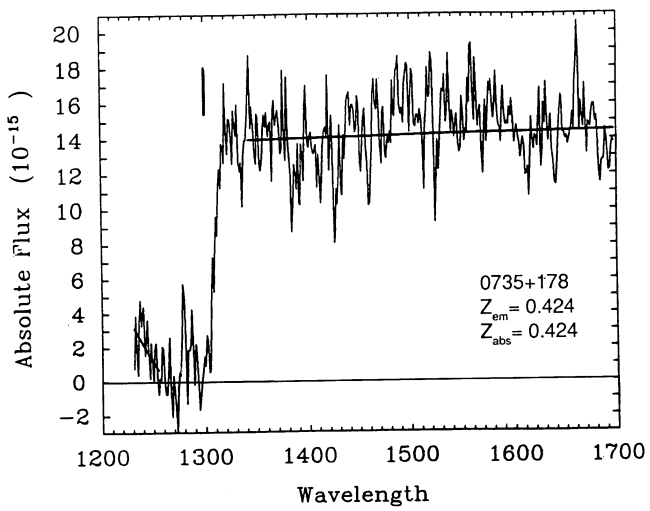

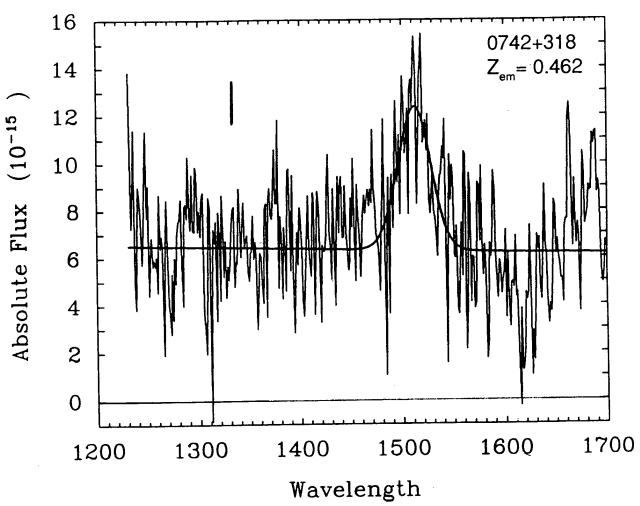

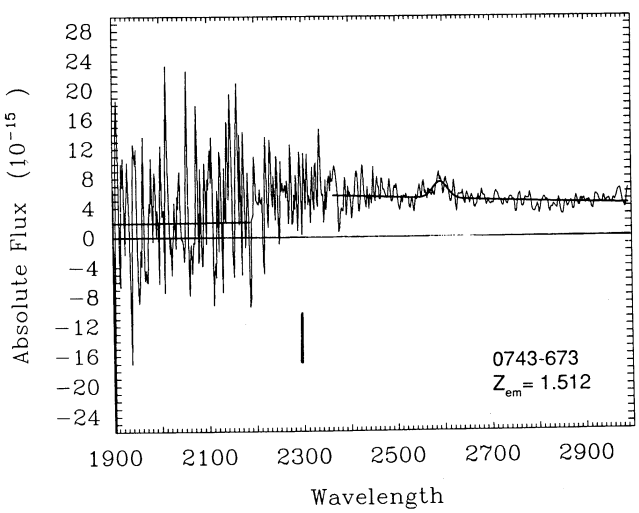

FIG. 2—*Continued*

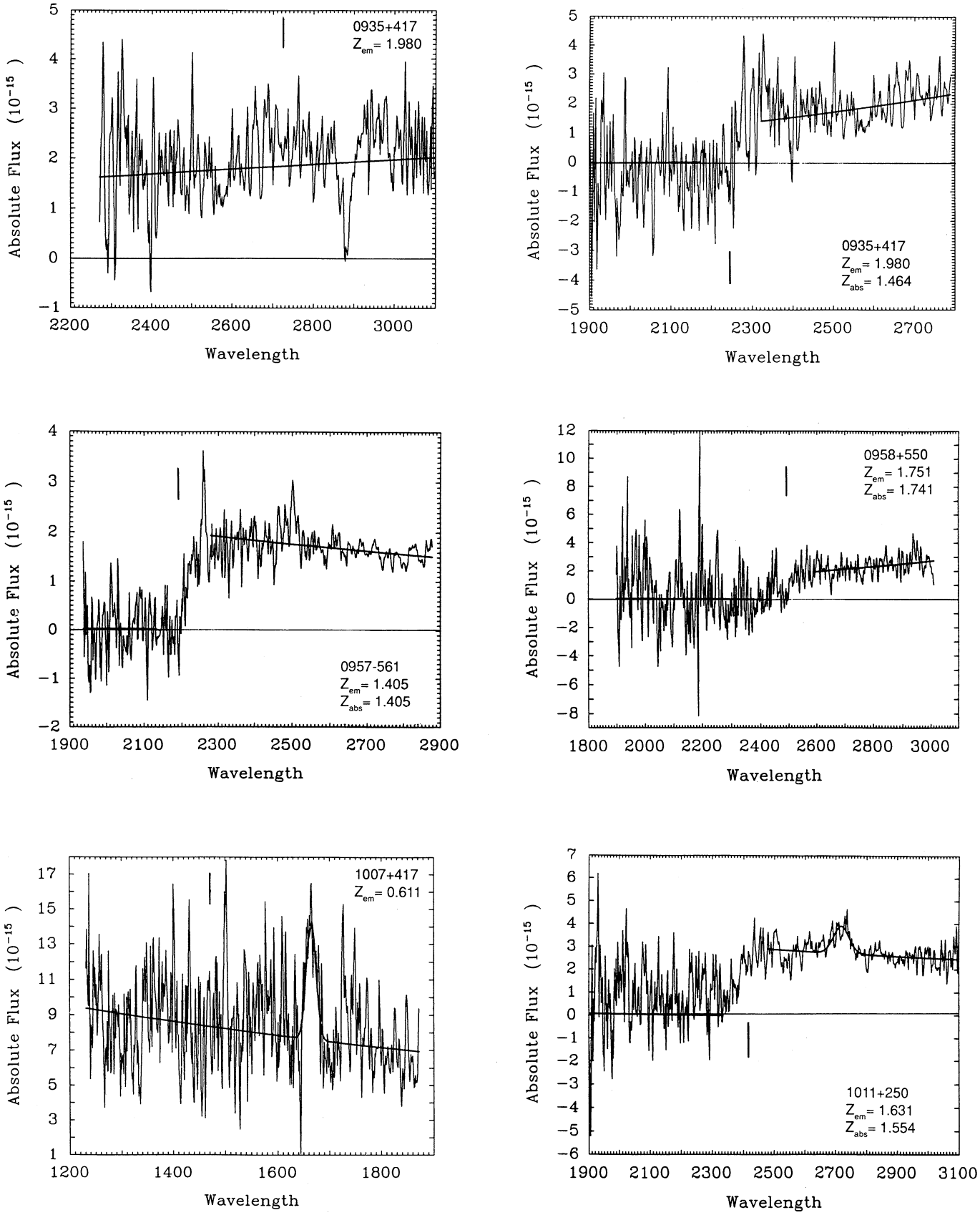

FIG. 2—*Continued*

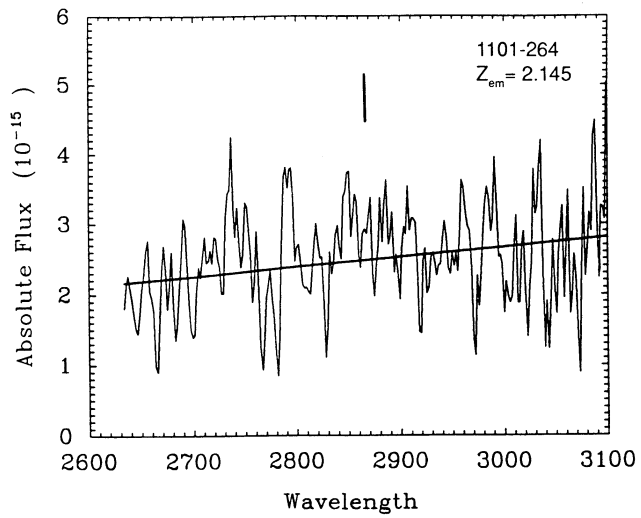

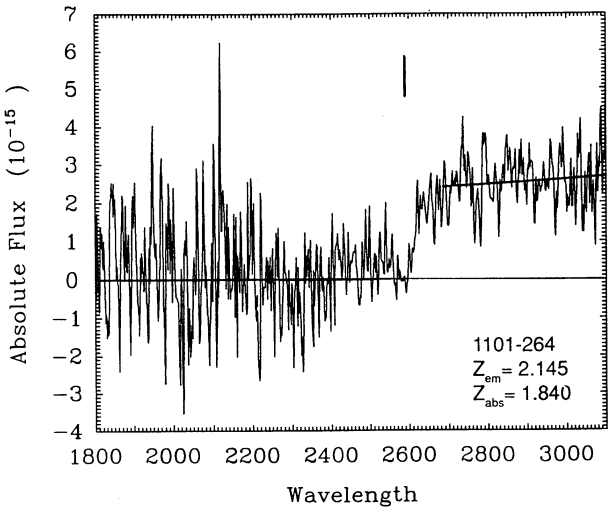

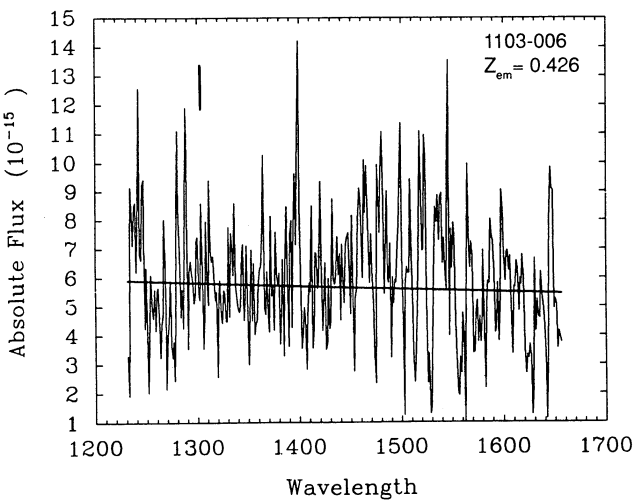

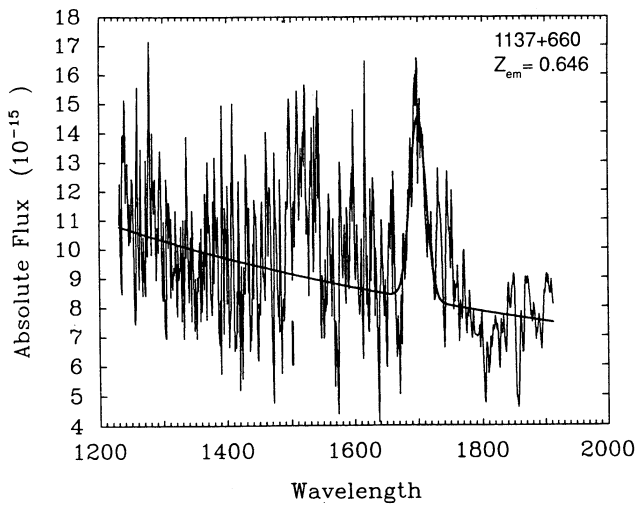

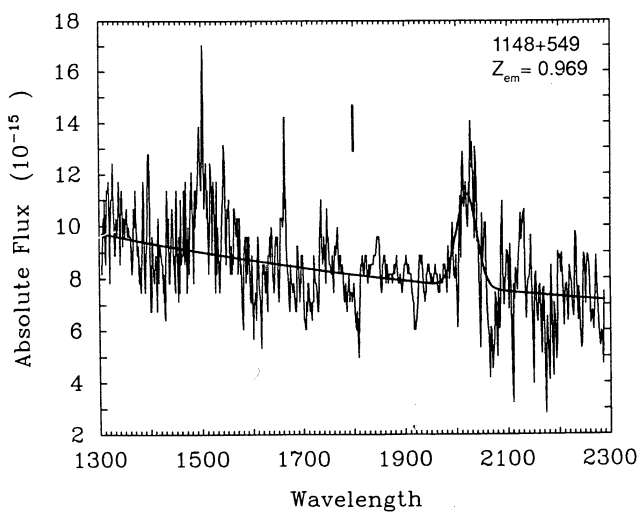

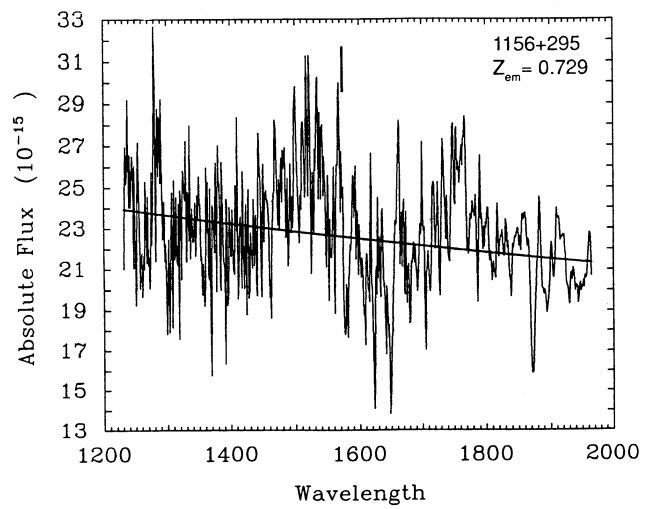

FIG. 2—*Continued*

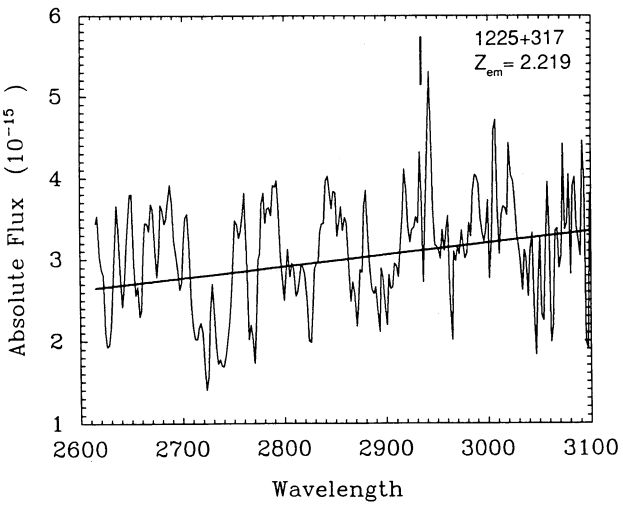

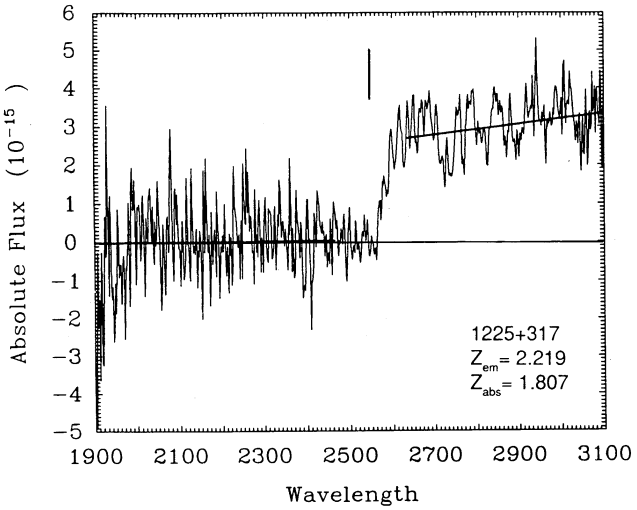

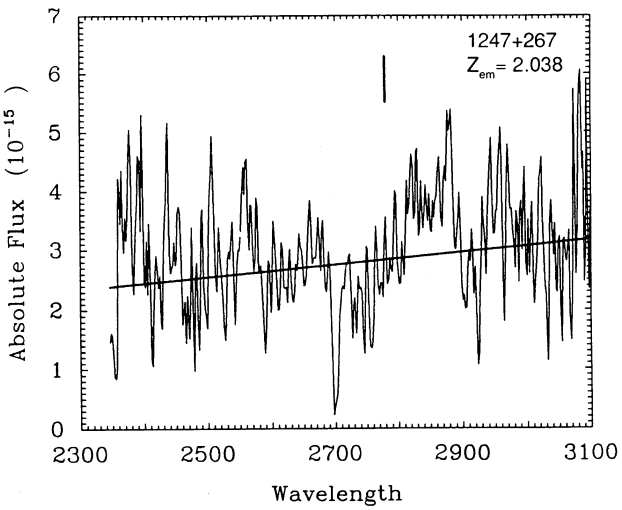

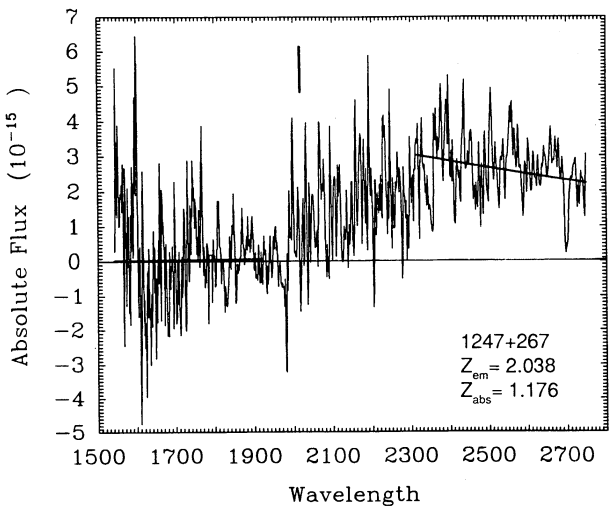

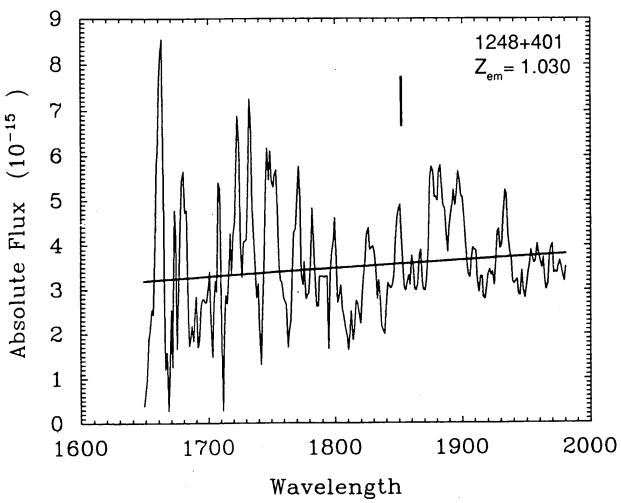

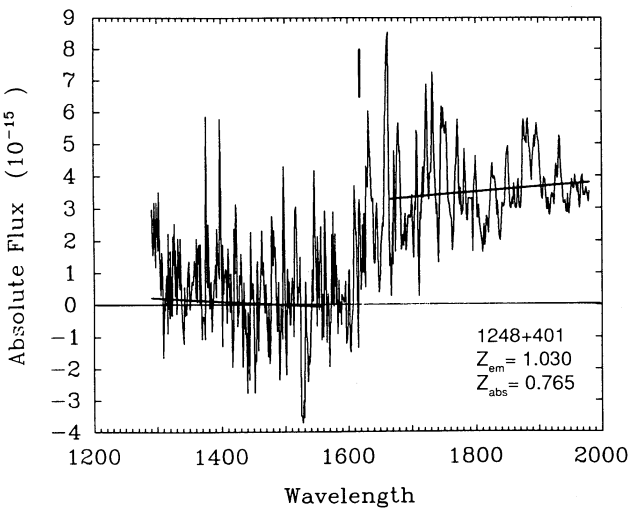

FIG. 2—*Continued*

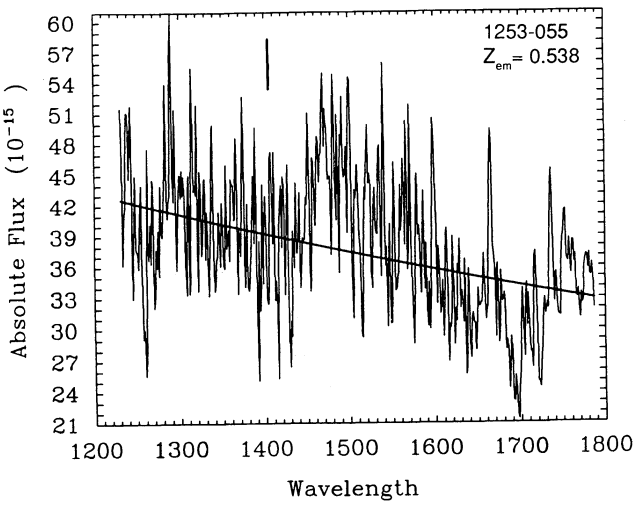

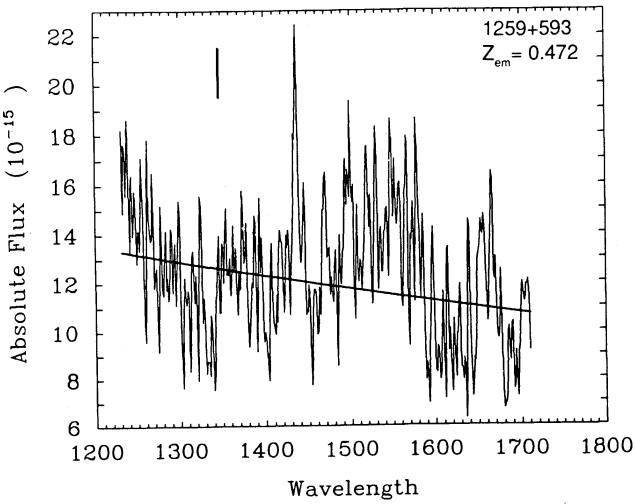

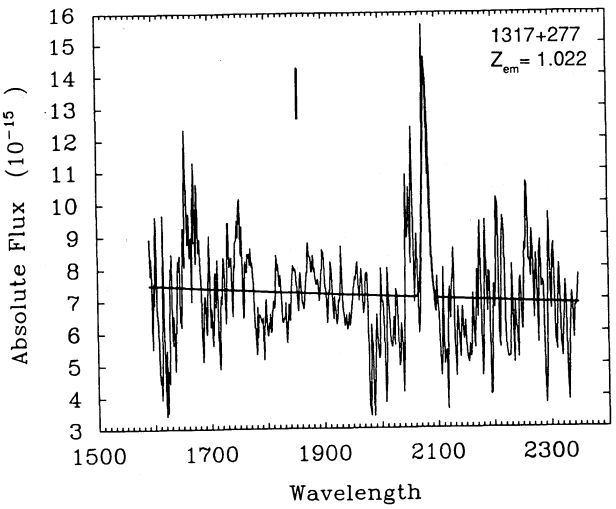

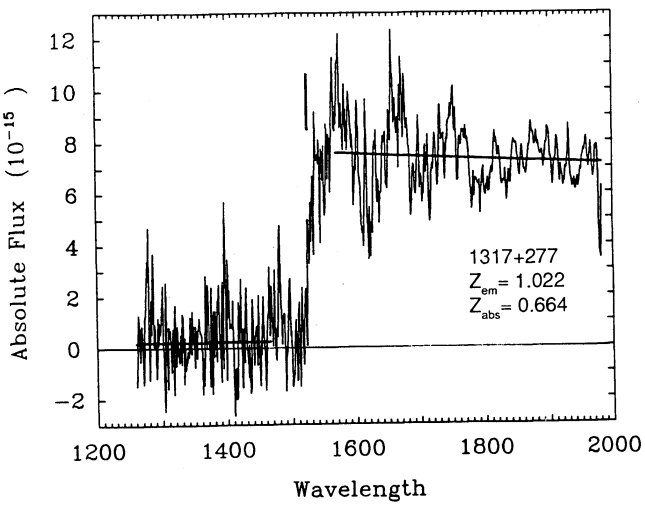

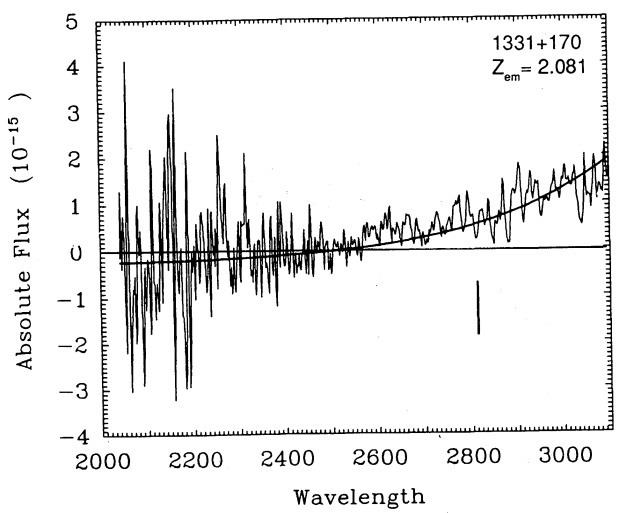

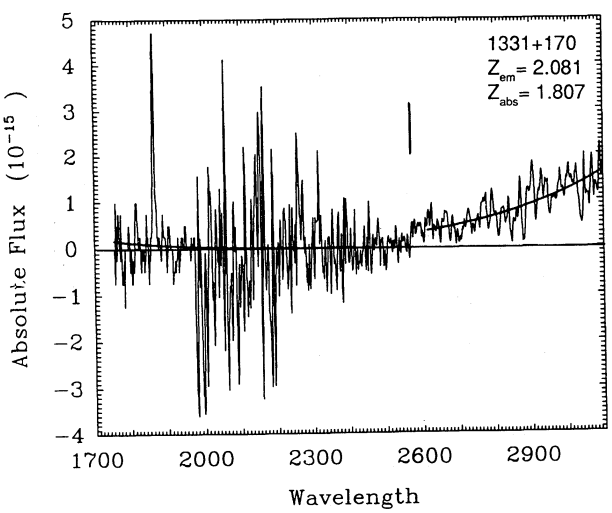

FIG. 2—*Continued*

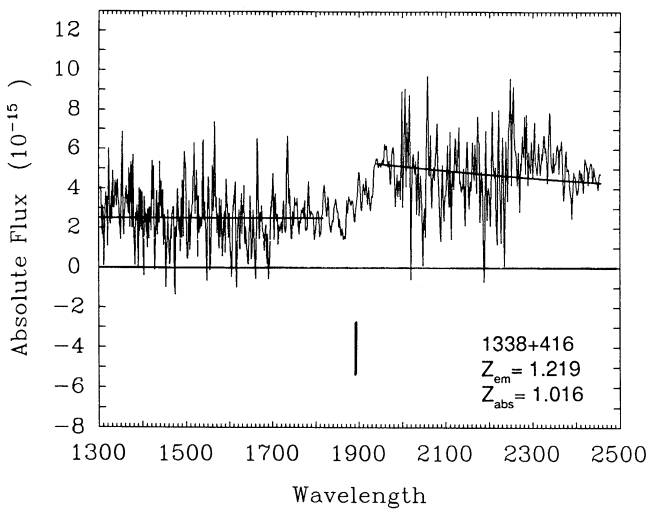

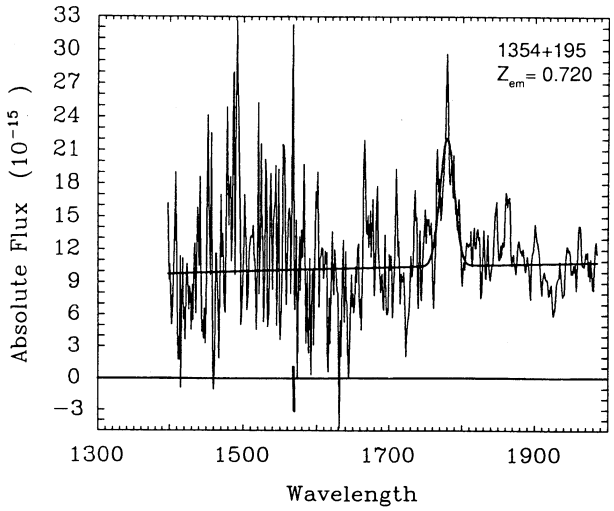

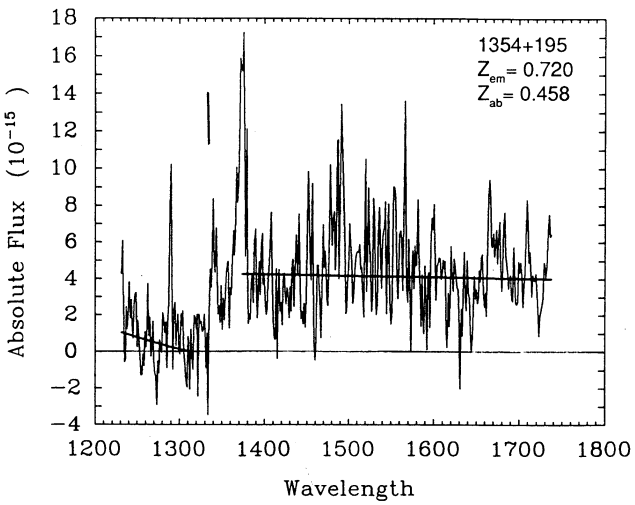

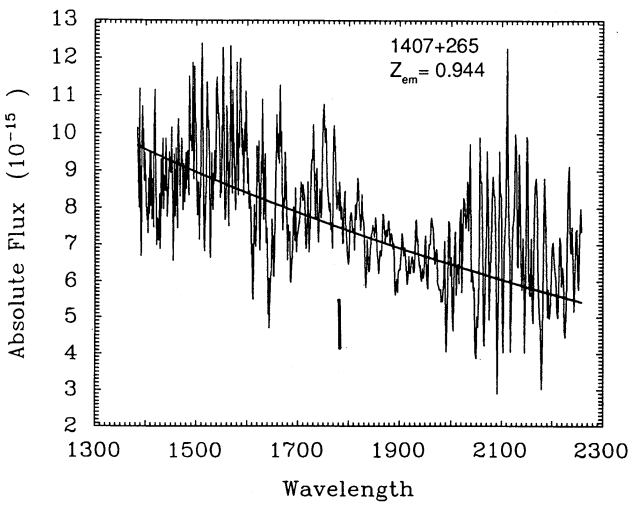

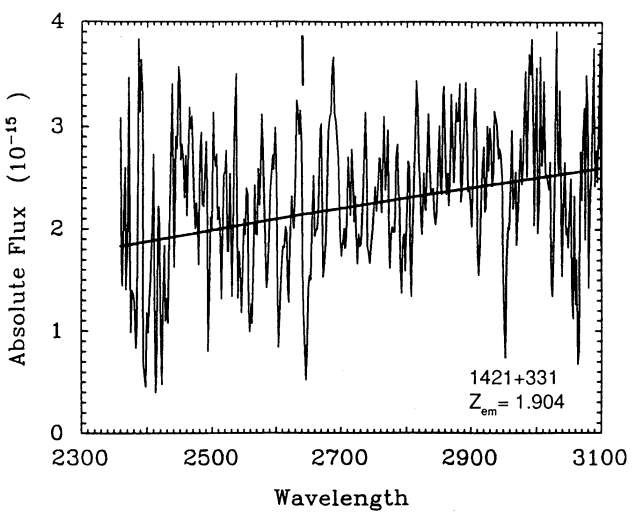

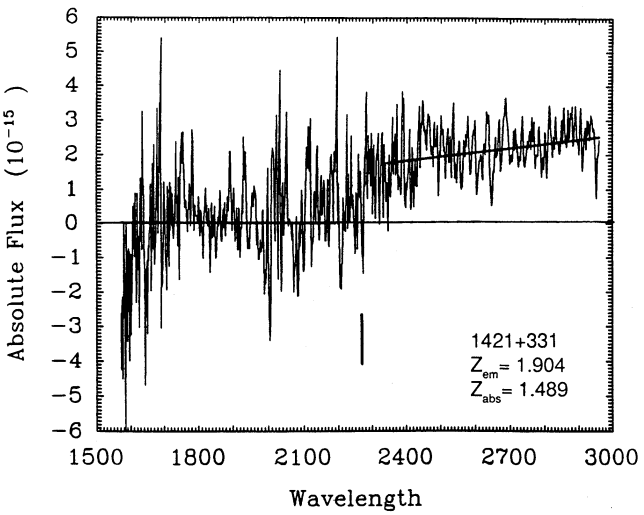

FIG. 2—*Continued*

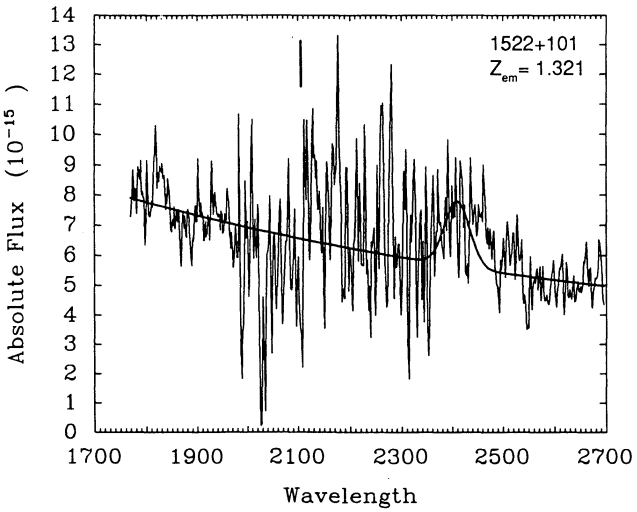

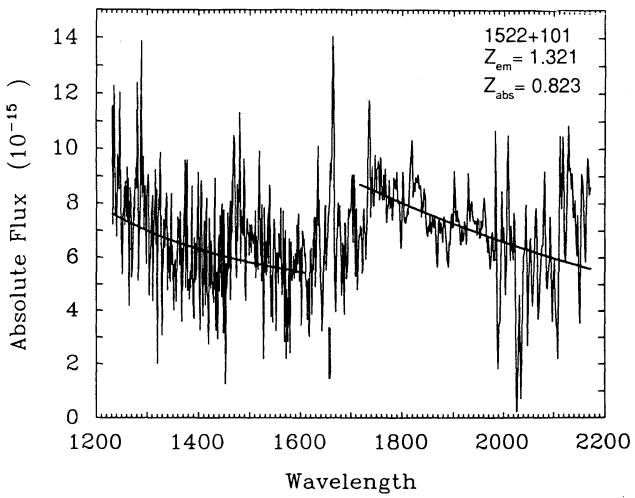

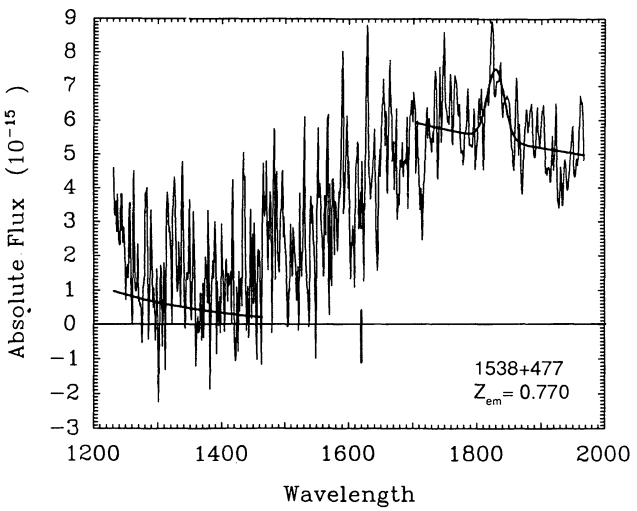

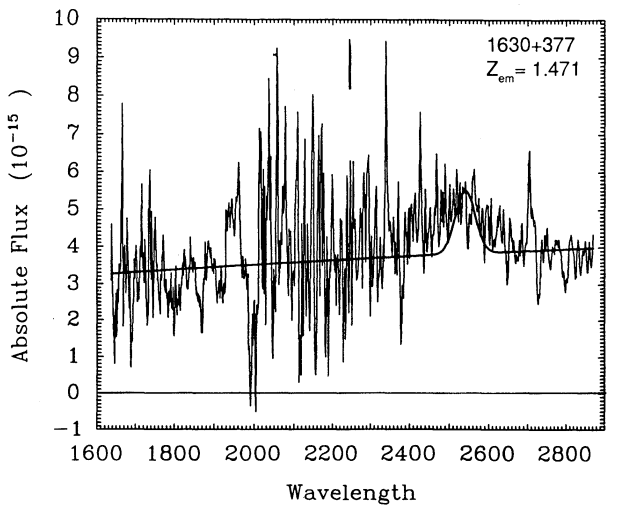

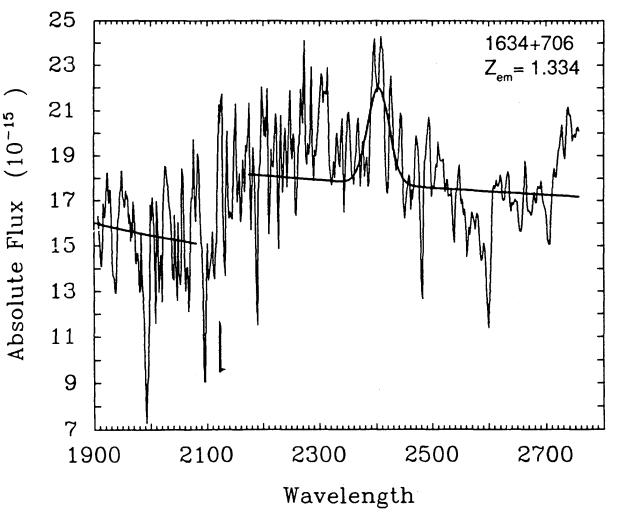

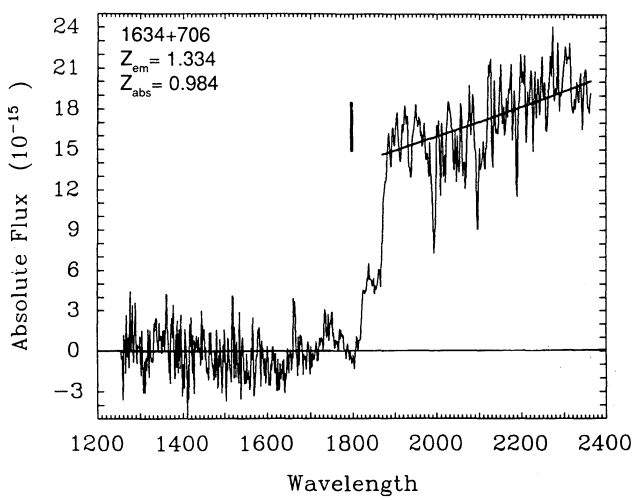

FIG. 2—*Continued*

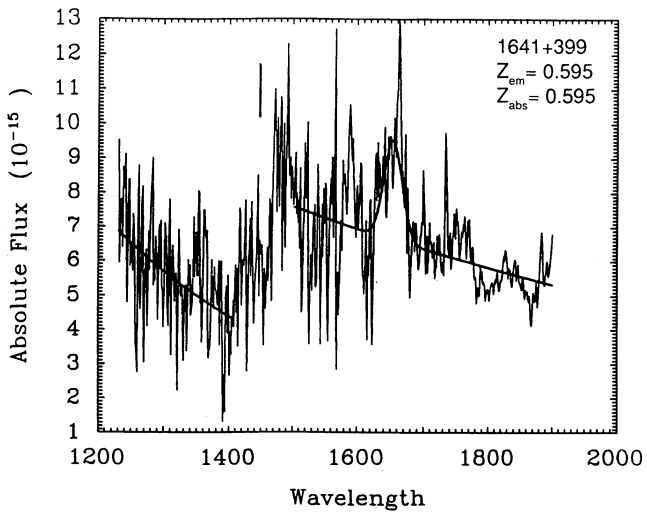

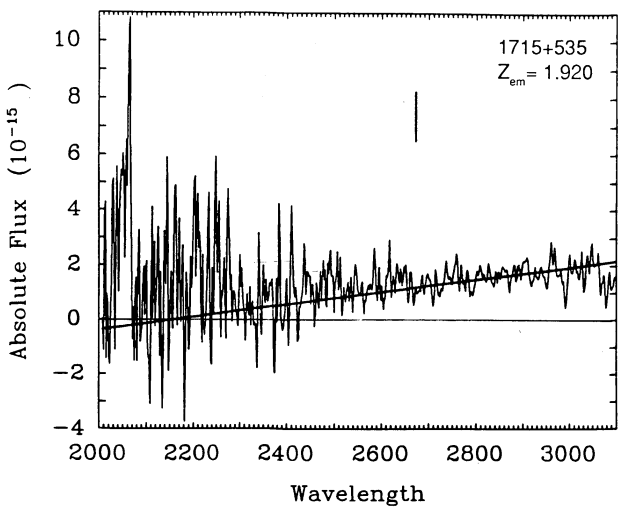

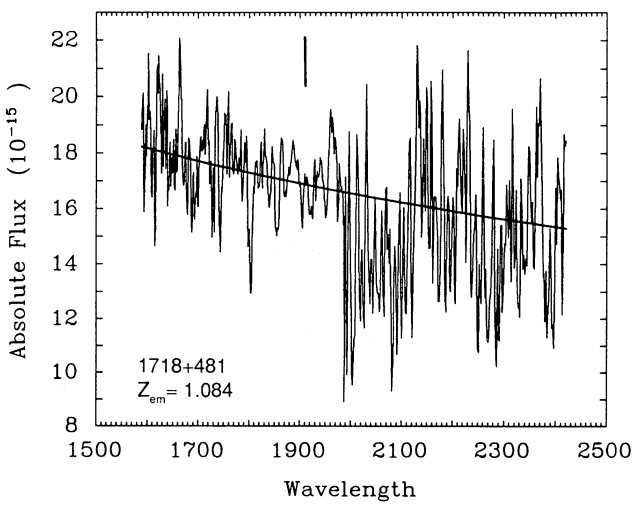

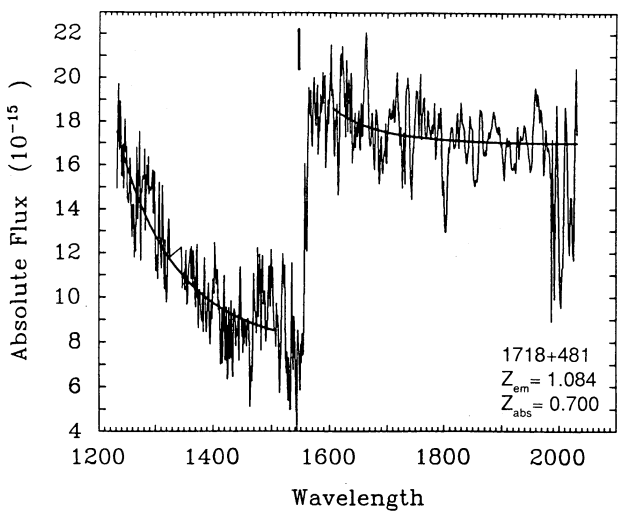

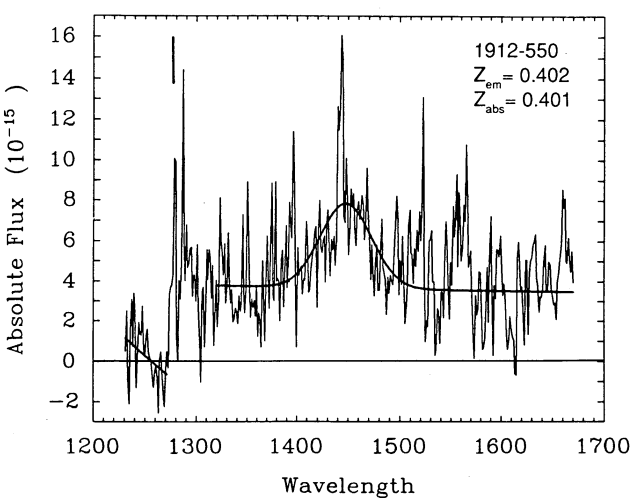

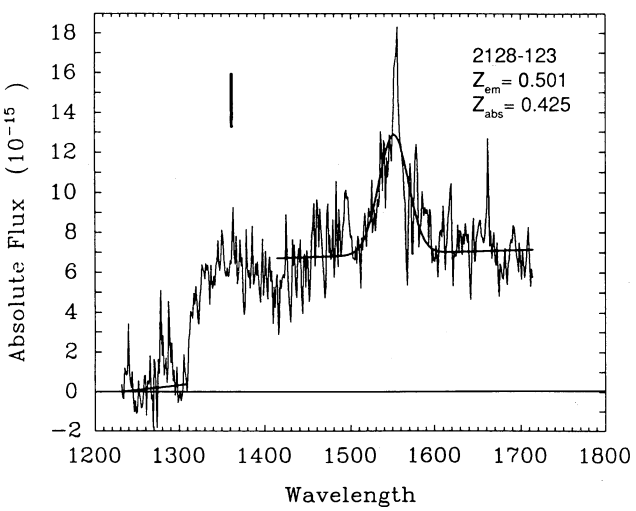

FIG. 2—*Continued*

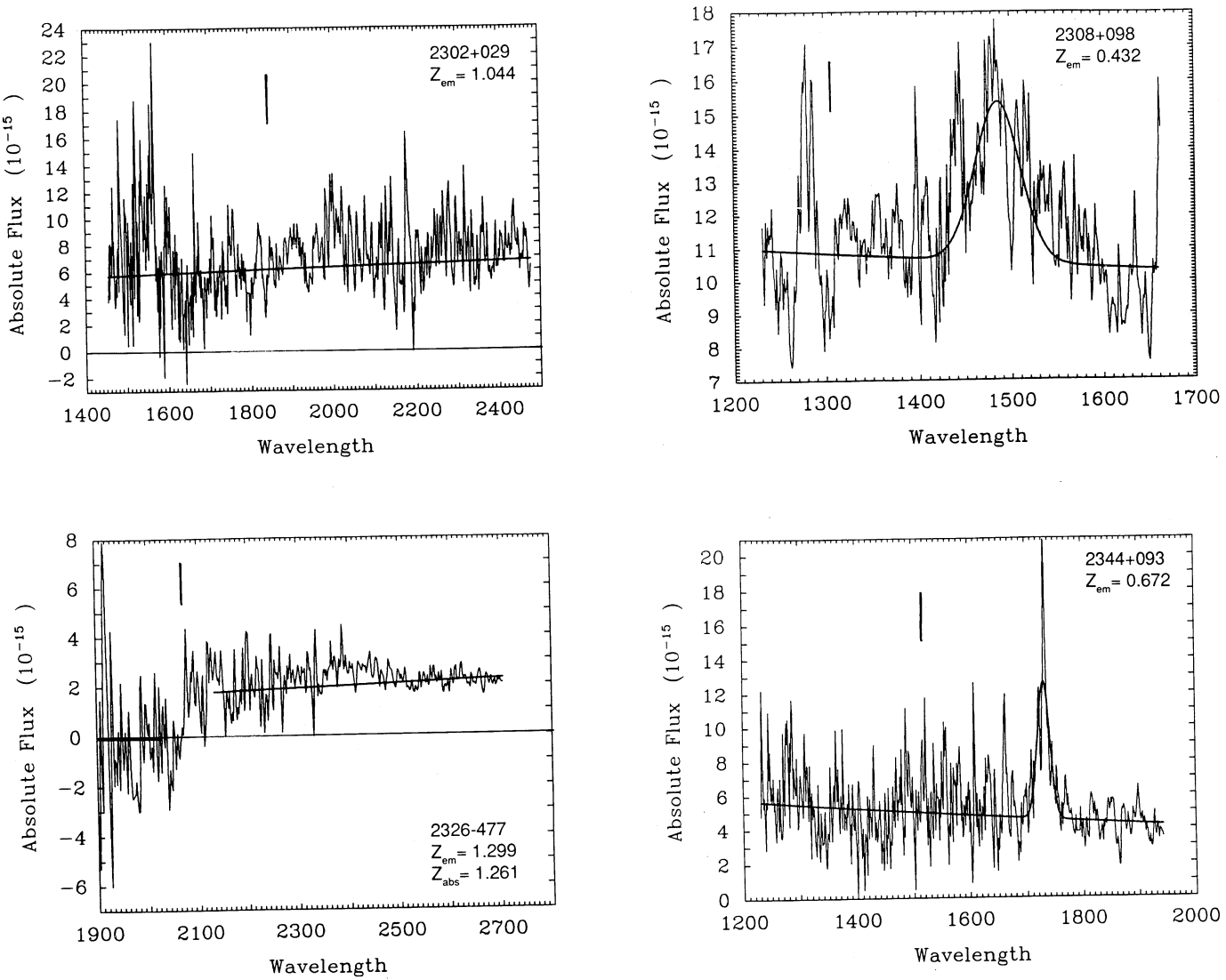

FIG. 2—*Continued*

well as at $z_{abs} \approx z_{em}$ and has been grouped with objects which show discontinuities at the systemic redshift with associated narrow Lyman and metal absorption lines, i.e., objects with $z_{abs} \approx z_{em}$.

3.3. *Group 3: Discontinuities at $z_{abs} \approx z_{em}$ and with Associated Narrow Lyman and Metal Absorption Lines*

This group consists of all objects with observed Lyman edge discontinuities with associated narrow absorption lines which are less than 20,000 km s^{-1} from the emission redshift of the quasar (see Table 4) and forms 22% of the sample. Table 4 includes the percentage discontinuities, their significance, references to absorption-line observations, the redshift at which the Lyman limit system is found, and the corresponding absorption line. Once again, discrepancies between the Lyman edge redshift and the absorption-line redshift are attributed to measuring error or due to blending of high n Lyman absorption lines.

3.4. *Group 4: Discontinuities at z_{em} With No Known Associated Narrow Lyman and Metal Absorption Lines*

This group forms 10% of the sample (see Table 5) and comprises our candidates for absorption by a thin accretion disk at the Lyman edge. The table shows the percentage discontinuity and its significance. Although 0743−673 shows Lyman edge discontinuity with very low significance, it is included in this group and not in group 1, because its spectrum has no known absorption-line systems affecting the continuum *and* the change in the slopes on either sides of 912 Å is significant.

4. DISCUSSION

4.1. *Nature of the Lyman Edges Observed in the Sample*

Most of the Lyman absorption edges in the $z_{abs} < z_{em}$ group (group 2; see Table 3) are not velocity broadened; and the flux goes down to zero in the region below the Lyman edge. For seven of the objects in group 2, the flux in the continuum below

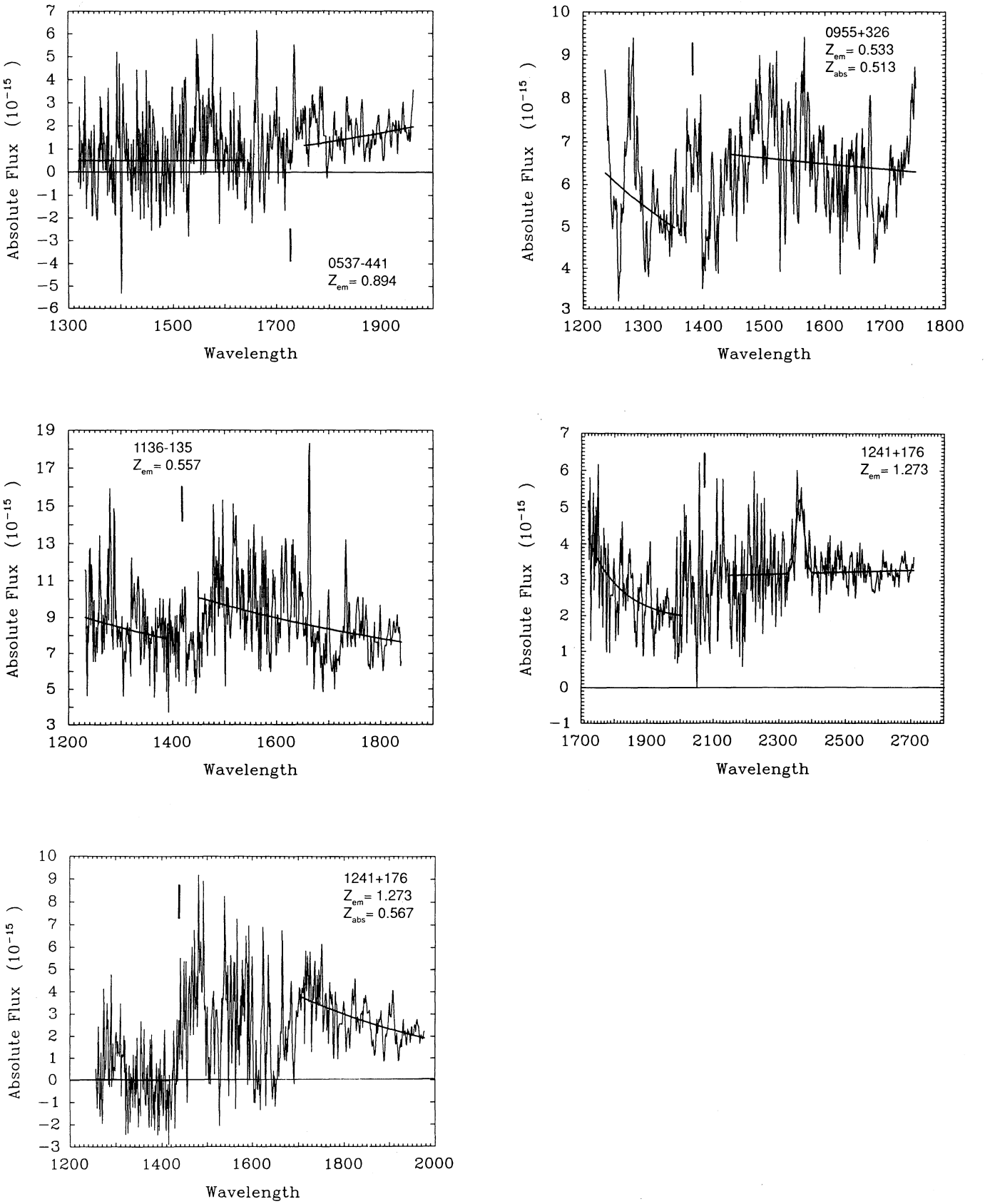

FIG. 3.—Continuum power-law fits to the objects which are "possible Lyman edge detections." These objects have been excluded from the analysis. The units of flux are ergs cm^{-2} s^{-1} $Å^{-1}$, and the observed wavelength is in angstroms. The position at which the systemic Lyman edge is expected is marked.

TABLE 3

LIST OF OBJECTS WITH $z_{abs} < z_{em}$

Object Name	D (%)	S(D)	z_{abs} (912 Å)	v/c	Line	z_{abs} Line	References	Other References
0002+051.....	103	26	0.845	0.42	Mg II	0.85	1	6
0237−233.....	82	6	1.632	0.20	Lyβ	1.63	2	
	...	...	...	...	C IV	1.635	3	1, 9, 11, 12
	...	...	...	...	Mg II	1.636	4	13
0935+417.....	99	12	1.464	0.19	C IV	1.464	1	
1101−264.....	100	43	1.840	0.10	C IV	1.839	5	11, 14
	...	...	...	...	Mg II	1.839	4	13
1225+317.....	98	36	1.807	0.14	Lyγ	1.796	2	12, 14
	...	...	...	...	Lyβ	1.796	2	12, 14
	...	...	...	...	Lyα	1.796	2	12, 14
	...	...	...	...	C IV	1.796	6	11, 12
	...	...	...	...	Mg II	1.796	7	15
1247+267.....	98	30	1.176	0.32	Lyα	1.22	2	9, 11, 16
1248+401.....	103	26	0.765	0.14	Mg II	0.773	1	
1317+277.....	97	60	0.664	0.19	Mg II	0.660	8	
1331+170.....	105	5	1.807	0.09	C IV	1.776	9	
	...	...	...	...	Mg II	1.776	4	7, 11
1354+195.....	104	16	0.458	0.16	Mg II	0.457	10	
1421+331.....	100	22	1.489	0.15	C IV	1.462	10	4, 7, 11, 17
1522+102.....	43	33	0.823	0.24	...	...		
1634+706.....	18	15	1.047	0.13	Lyγ	1.046	2	
	...	...	...	...	Lyβ	1.046	2	
	...	...	...	...	Lyα	1.046	2	
	...	...	...	...	Mg II	1.046	1	
	100	123	0.984	0.16	Mg II	0.993	1	
1718+481.....	59	63	0.700	0.20	Mg II	0.713	1	

REFERENCES—(1) Bechtold et al. 1984; (2) this paper; (3) Boroson et al. 1978; (4) Lanzetta, Turnshek, & Wolfe 1987; (5) Petitjean & Bergeron 1990; (6) Young, Sargent, & Boksenberg 1982a; (7) Caulet 1989; (8) Tytler et al. 1987; (9) Sargent, Boksenberg, & Steidel 1988; (10) Weymann et al. 1979; (11) Young, Sargent, & Boksenberg 1982b; (12) Sargent et al. 1980; (13) Boisse & Bergeron 1985; (14) Carswell et al. 1982; (14) Snijders, Pettini, & Boksenberg 1981; (15) Bechtold, Boron, & York 1987; (16) Green et al. 1980; (17) Foltz et al. 1986.

TABLE 4

LIST OF OBJECTS WITH $z_{abs} \approx z_{em}$

Object Name	D (%)	S(D)	z_{abs} (912 Å)	v/c	Line	z_{abs} Line	References	Other References
0215+015.....	73	40	1.715	0.000	Lyα	1.719	1	
					Lyβ	1.649	1	
	99	14	1.346	0.145	C IV	1.344	1	
					Mg II	1.344	2	8
0302−223.....	100	17	1.330	0.030	Lyα	1.330	3	
					Lyβ	1.330	3	
0454−220.....	100	58	0.486	0.032	Lyα	0.480	3	
					Mg II	0.483	4	
0735+175.....	126	88	0.424	0.000	Lyα	0.424	3	
					Mg II	0.424	5	
0957+561.....	95	21	1.405	0.000	Lyα	1.390	3	
					Mg II	1.390	6	8, 13
0958+550.....	103	13	1.741	0.006	C IV	1.730	7	13
					Mg II	1.732	8	9
1011+250.....	101	35	1.554	0.030	C IV	1.599	9	13, 14
1641+399.....	52	26	0.595	0.000	C IV	0.595	3?	
					Ca H, K	0.59	10	
1912−550.....	125	8	0.401	0.001	C IV	0.401	3	11
2128−123.....	89	36	0.425	0.052	Lyα	0.42	3	11
					Mg II	0.43	11	4, 12, 13
2326−477.....	108	10	1.261	0.017	Lyα	1.26	3	
					Mg II	1.26	12	

REFERENCES—(1) Blades et al. 1985; (2) Blades et al. 1983; (3) this paper; (4) Tytler et al. 1987; (5) Boksenberg, Carswell, & Sargent 1979; (6) Bechtold et al. 1984; (7) Sargent, Boksenberg, & Steidel 1988; (8) Caulet 1989; (9) Foltz et al. 1986; (10) Ellingson, Green, & Yee 1991; (11) Bergeron & Kunth 1983; (12) Petitjean & Bergeron 1990; (13) Weymann et al. 1979; (14) Young, Sargent, & Boksenberg 1982b.

TABLE 5

LIST OF POSSIBLE CANDIDATES

Object	D	S(D)	Comments and Caveats
0117+213.....	95	12	0.44%–0.61% polarization Flat Lyα, complete discontinuity
0405−123.....	24	101	≤1% polarization; Lyman edge is not velocity broadened
0743−673.....	10	4	≤1% polarization
1338+416.....	44	22	Possible Lyα absorption
1538+447.....	99	44	Velocity dispersed edge

Lyα is decreasing toward short wavelengths, indicating possible Lyman absorption lines which cannot be distinguished due to the low S/N and resolution (Steidel & Sargent 1987; O'Brien et al. 1988). The narrow absorption lines corresponding to the Lyman edges are not within the emission-line width, indicating that the gas responsible for the absorption is not in the emission-line region of the quasar. The gas responsible for absorption is extrinsic to the AGN and its host galaxy. It could be, for example, intervening galaxy halos and intergalactic gas.

The absorption edges observed for the objects in the $z_{abs} \approx z_{em}$ group with associated Lyα, or metal (C IV λ1549, Mg II λ2798) absorption lines are not velocity broadened (group 3; see Table 4 for objects and references). Intervening clouds not only show a Lyman edge but also narrow absorption lines of Lyα, C IV, or Mg II. Therefore, the absorbing gas in this group of objects can be (1) material associated with the emission line region of the quasar, (2) material ejected from the quasar, (3) interstellar medium of the host galaxy or a companion galaxy, (4) gas in the cluster to which the quasar belongs, or (5) intergalactic medium not associated with the quasar or its environment.

The Lyman edge discontinuities for the objects in the $z_{abs} \approx z_{em}$ group with no associated narrow Lyman and metal absorption lines (group 4; see Table 5) are possible candidates for testing accretion disk models. The objects in the $z_{abs} \approx z_{em}$ group with associated narrow Lyman and metal absorption lines (group 3), are not considered as possible accretion disk candidates for the following reason. If the absorption lines in these objects are due to disk material, we expect the absorption features to be at least as broad as the quasar emission lines because of the large gas velocities in the disk. Such broad absorption features are not seen. Hence, only the objects in the $z_{abs} \approx z_{em}$ group *without* associated narrow absorption lines are considered as possible candidates for testing accretion disk models.

4.2. *Lyman Edges from Accretion Disks: Comparison of Predictions with Observations*

Simple models of optically thick, geometrically thin accretion disks predict significant Lyman absorption at 912 Å in the quasar rest frame (Kolykhalov & Sunyaev 1984), yet most observations of quasars do not show a Lyman edge. To account for a weak Lyman edge, Sun & Malkan (1989a, b) argued that the absorption at 912 Å weakens as the disk surface gravity is lowered (see their Fig. 1); they also pointed out that the strength of the absorption feature depends on the inclination angle of the accretion disk because of Doppler broadening. Taking into account both the surface gravity and the inclination angle, the Sun and Malkan models predict discontinuities up to 80% at the Lyman limit. The face-on disks show a dominant Lyman absorption feature, while the edge-on disks hardly show an edge. Laor & Netzer (1989) consider a full treatment of electron and bound-free opacities in their calculations and predict an emission feature at the Lyman edge depending on the inclination angle (see their Fig. 4). Laor's (Laor & Netzer 1992) disk models also predict that the Lyman edge would be shifted in wavelength due to the gravitational field of the central supermassive black hole, and Lyman edge would be velocity broadened depending on the inclination angle. Czerny & Pojmanski (1990) considered the effect of density in their calculations and showed that Lyman edges can be either in absorption or emission for a broad range of parameters.

In any thermal model, there will be some feature at 912 Å, since the opacity of the gas changes dramatically. Therefore, the shape of the continuum around the Lyman limit is a discriminant between optically thick thermal models and nonthermal models. The Lyman edge discontinuity has not yet been calculated for geometrically thick disk models. In thick disk models, since the effective surface gravity is very small, the discontinuity is also expected to be smaller than in thin disk models. However, in the limit a thick accretion disk would have a spectrum very similar to a star of the same effective temperature and near zero gravity, and a Lyman edge feature should be seen at 912 Å. The Lyman edge feature can be weakened if the hotter parts of the disk produce an emission feature while the cooler parts produce an absorption feature. Another possibility is that the accretion disk is heated from above the disk. This heating results in a feature at the Lyman limit in emission for certain parameters. Yet another possibility is scatter broadening the edge feature (Czerny & Zbyszewska 1991), but this aggravates the polarization observations (see Antonnuci 1991).

To obtain observational evidence for accretion disks, we are only interested in discontinuities at the quasar emission redshift that have no evidence of corresponding narrow absorption lines. In the sample, the only objects that can be considered to show any evidence for accretion disks are those that belong to group 4. See § 4.1 for details of why the $z_{abs} \approx z_{em}$ group cannot be used for testing accretion disk theory.

If we assume that all the discontinuities seen in group 4 are due to accretion disks, then models predict that ≈70% of AGNs should show discontinuities (≥20%) for randomly distributed viewing angles. In our sample, 10% of the AGNs show discontinuities; of these, only 1538+447 has a discontinuity broad enough to be caused by an accretion disk. A discontinuity weaker than 15% cannot be detected because of poor S/N. Therefore, the observations and theory can be consistent only if most discontinuities are ≤15%.

Since the accretion disk is closer to the supermassive object than the BLR clouds, the Lyman edge discontinuity can be highly velocity dispersed below Lyα due to gravitational effects. In this picture, the slope of the continuum in the wave-

length region below Lyα would differ from the slope of the continuum longward of Lyα. To check if any such velocity-broadened Lyman edges have been missed, group 1 objects were investigated for continuum decreasing toward shorter wavelengths. Only four objects (0454+039, 1630+377, 1715+535, 2302+029) show steepening of the continuum slope at wavelengths below Lyα compared to the continuum slope at wavelengths above Lyα. This result does not contradict the observations by O'Brien et al. (1988) because the amount of steepening in the Lyman continuum is a function of redshift. In 0454+039 and 1715+535, metal absorption lines at redshifts less than the quasar redshifts have been observed (Weymann et al. 1979; Petitjean & Bergeron 1990; Caulet 1989; Sargent, Boksenberg, & Steidel 1988). Narrow Lyman absorption lines corresponding to the metal absorption-line systems might be causing the decline in the continuum, but the S/N in the spectra is insufficient to detect such absorption features. A Lyman edge corresponding to the absorption systems is detected at a very low significance level for both these quasars. No change in the slope of the continuum above and below Lyα is present in 2302+029. For 1630+377, we do not have any observations for wavelengths greater than Lyα in the *IUE*. It can be concluded that at most three more AGNs (6%) of the sample show velocity-broadened Lyman edges apart from the objects in group 4.

The strength of the Lyman edges can be much smaller than predicted by accretion disks, if the disk is heated from above. In this scenario, external heating could also drive the edge into emission. Then, depending on the inclination angle, some of the AGNs should show emission discontinuities. No emission discontinuities greater than $\approx 15\%$ are observed in the sample. In fact, to our knowledge no Lyman edge emission has been reported in any quasar.

As discussed above, the nature of the Lyman edge can be affected by the strong gravitational field of the central black hole. In edge-on disks the Lyman edge is smeared out in wavelength and is blueshifted with respect to the emission redshift of the quasar (Sun & Malkan 1989; Laor & Netzer 1992). Hence, in edge-on disks the Lyman edges are velocity broadened and appear to be weak. In the case of the face-on disks, the Lyman edge discontinuities are not strongly velocity broadened and appear sharper. We have investigated a region ≈ 500 Å around 912 Å. Any feature greater than 15% in this region is detectable over most of the region. Yet, the observed number of discontinuities are small. If the low incidence of Lyman edges in our sample is consistent with geometrical aspects of the accretion disk theory, accretion disks cannot be randomly oriented to the line of sight but are all close to edge-on!

If the Lyman edges observed in our sample have to be consistent with the predictions of the optically thick, geometrically thin accretion disk models, then (1) most Lyman edge features either in absorption or emission have to be $\leq 15\%$ or (2) the accretion disks are not randomly oriented to the line of sight, but are preferentially edge-on.

4.3. *Lyman Edges from BLR Clouds: Comparison of Predictions with Observations*

To understand the geometry and nature of the BLR clouds, we are only interested in discontinuities at the quasar emission redshift (i.e., groups 3 and 4). Therefore, objects in groups 1 and 2 can be grouped together as objects which show no intrinsic Lyman edge discontinuity.

For some of the objects in groups 3 and 4 the nature of the intervening gas has been studied in detail. For example, 1912−550 has been imaged by Bergeron & Boisse (1986) and the intervening companion galaxy, which is the source of the absorption, has been identified. Similarly, 1011+250, 1641+399 (Ellingson, Green, & Yee 1991) and 2128−123 (Bergeron 1986) have absorption edges from companion galaxies. The narrow Lyα absorption lines in 0215+015, 0302−223, and 0957+561 show complete absorption of both the emission-line photons as well as the continuum photons, indicating that the absorbing gas is not associated with the BLR. Lanzetta (1988) concluded that Lyman limit systems are consistently being generated by intervening intergalactic gas. In comparison to Lanzetta (1988), we see a small excess (by a factor of 3) of absorption edges (partial and complete) at the systemic redshift for the low redshift objects in our sample. This provides some evidence that at least some of the Lyman edges are due to absorption gas intrinsic to the quasar. Thus, in our sample only nine AGNs (16%) show evidence for possible absorption due to BLR clouds. Of these nine AGNs, five show complete Lyman edge absorption, and the remaining four show partial Lyman edge absorption.

If the 16% discontinuities in the sample are due to BLR clouds, we can determine the distribution of the BLR clouds (i.e., the geometry) and the cloud size relative to the source size. There are three possible cases.

In the first case, the size of the BLR clouds is similar to that of the source and the clouds are distributed randomly around the source. In this scenario, some of the clouds must lie along the line of sight to the continuum source and would give rise to strong absorption at the Lyman limit, in Lyman absorption lines, and in absorption lines of abundant metals like C IV and Mg II. In this case, the fraction of quasars showing Lyman limit absorption would give the covering factor, i.e., the typical fraction of the continuum source covered by extended emission-line region clouds. A covering factor of $\approx 10\%$ is derived from counting the number of ionizing photons and comparing with the number of Lyα photons. This would predict that 90% of the quasars should have no discontinuity, while 10% should have some discontinuity. For the present sample, observations show that 10% of the quasars have complete discontinuities at the quasar Lyman edge, but there are also 6% of the quasars with partial discontinuities. Assuming that all the discontinuities are due to BLR clouds the average covering factor is 11% assigning partial weights to partial discontinuities. This is similar to that derived from the number of ionizing photons.

In the case of BLR cloud size larger than the continuum source size, the nature of the clouds can be investigated if the discontinuities in the sample objects are due to BLR clouds. Most BLR clouds are thought to have column densities of $\approx 10^{22}$ cm^{-2} (Kwan & Krolik 1981). But if the clouds are large compared to the continuum source, such large column densities would lead to damped Lyα absorption systems (damped systems are seen for column densities $\geq 10^{21}$ cm^{-2}) as well as complete absorption at the Lyman edge. The observations do not show complete Lyman edges accompanied by damped Lyα systems. Therefore, the column densities of the absorbers must be less than 10^{21} cm^{-2}. If the absorption is due to BLR clouds, the column densities of these clouds are lower than considered previously.

In the second scenario, the BLR cloud size is much smaller than the central source, and the clouds are distributed randomly around the source. In this case, the BLR clouds cover only a

part of the central source, and every line of sight will have Lyman edge absorption due to the clouds which is partial because some of the radiation from the central source is directly observed. The amount of absorption will depend on the amount of obscuration due to the BLR clouds, i.e., on the covering factor. The amount of absorption at the Lyman edge would be equal to the covering factor. The Lyman edge discontinuity would be velocity broadened by the velocity distribution of the BLR clouds, which is similar to the width of the BLR emission lines. In this scenario, all quasars will have partial discontinuities, and the amount of discontinuity would be equal to the covering factor. Since the covering factor is $\approx 10\%$ and the detection limit of the data is 15%, this scenario at a first glance seems quite consistent with the observations. In the present sample, 10% of the quasars which show complete discontinuities cannot be easily explained unless the discontinuities are due to intervening companion galaxies. A systematic search will determine the nature of the discontinuities.

In the third scenario, the BLR clouds are distributed in a disk geometry. In this picture, the lines of sight perpendicular to the disk are not obscured, but the lines of sight along the disk are obscured. The amount of obscuration at the Lyman edge would depend on the column density of the absorbers in the line of sight, i.e., the number of BLR clouds intervening in the line of sight. The velocity width of the Lyman edge will be similar to the velocity width of the BLR clouds projected on the line of sight. In this case, some objects would show Lyman edge emission because some of those photons are scattered into the line of sight. Some objects would show no Lyman edges because the line of sight is not in the plane of the BLR disk. Some objects would show partial Lyman absorption edges because the distribution of BLR clouds in the line of sight is such that the column density is low. Finally, some objects would show complete absorption at the Lyman edge because the line of sight is nearly in the plane of the disk formed by the BLR clouds (see Carswell & Ferland 1988). The sample shows that 6% of the objects have partial edges, 10% have complete edges, and 70% have no discontinuities. The remaining 14% of the sample definitely have absorption at 912 Å not associated to the BLR clouds. This distribution of Lyman edges is easily explained by the disk geometry of the BLR clouds. The sample shows no Lyman edges in emission, indicating that the geometry of the BLR clouds is such that no line of sight has Lyman edge photons scattered into it, i.e., the plane of the BLR disk plane is not close to face-on.

If the intrinsic Lyman edges observed in our sample are due to BLR clouds, then (1) the cloud column densities are not as high as previously suggested for cloud sizes larger than the continuum source size and (2) both randomly distributed small clouds around the central source and a disklike geometry of the BLR are consistent with the observations.

5. CONCLUSIONS

A uniform search for Lyman edges in quasars, in the redshift range 0.4–2.3 using the *IUE* archives shows that

1. Thirty-nine percent of the sample do not show any discontinuities.
2. Twenty-nine percent of the sample show complete Lyman edges at redshifts less than the quasar redshift. These objects have associated narrow absorption lines, and hence the intervening gas responsible for the absorption is extrinsic to the quasar and its environment.
3. Twenty-two percent of the sample show Lyman edges at the quasar redshift with associated narrow absorption lines. In these objects the gas is associated with the AGN or its host galaxy.
4. Ten percent of the sample have Lyman edges with no known associated absorption lines. These are our candidates for accretion disk models, but these objects have not yet been systematically searched for associated absorption lines. Such a search would be necessary to make these into strong candidates.
5. If Lyman edge discontinuities are due to optically thick, geometrically thin accretion disks, which are randomly oriented to the line of sight, these results indicate that the Lyman edge discontinuity, either in emission or absorption, has to be $\leq 15\%$ in most quasars. The Lyman edge discontinuity may never be significant in emission.
6. If the Lyman edges are due to BLR clouds, then the cloud column densities are not as high as previously suggested for cloud sizes larger than the continuum source size. Also, both randomly distributed small clouds around the central source and a disklike geometry of the BLR are consistent with the observations.

The authors would like to thank G. Lee, R. R. J. Antonucci, and J. Pringle for their discussions and suggestions, and Dave Paradise in the art department for all the help with the many figures. This work was conducted under the NASA grant NAG5-1652.

APPENDIX A

FACTS ABOUT SOME INDIVIDUAL OBJECTS

1. 0002+051 ($z_{em} = 1.899$)

This object has a known absorption-line system at $z_{abs} = 1.744$ (Young, Sargent, & Boksenberg 1982). The Lyman limit and the high n Lyman lines of this $z_{abs} = 1.744$ absorption system would not allow us to detect an intrinsic Lyman edge at $z_{em} = 1.899$. Complete Lyman edge absorption is seen at $z_{abs} = 0.845$. The declining slope of the continuum toward smaller wavelengths is probably due to absorption by the Lyman series of the $z_{abs} = 1.744$ and 0.845 systems and the Lyα forest lines (Blades et al. 1985).

2. 0.117+213 ($z_{em} = 1.493$)

The discontinuity in this object appears to go to zero within ~ 150 Å of the Lyman edge. Since accretion disk models predict partial discontinuities, 0117+213 is not a viable candidate for an edge originating from an accretion disk. Possible additional absorption features are detected at 2400 Å and at 2840 Å, which correspond to Lyα and Lyβ at $z = 1.34$. The discontinuity observed

is possibly associated with the absorption at z of 1.34. Yet this object is listed in Table 5 as a possible candidate because the absorption system at 1.34 is not confirmed.

3. 0215+015 (z_{em} = 1.715)

The well-observed complex absorption features seen between the Lyα emission line and the Lyman edge at 912 Å have been investigated by Blades et al. (1983, 1985). We have not taken into account the absorption features in the fit presented in Figure 2. Nevertheless, the fit correctly shows a partial discontinuity at z_{abs} = 1.715 associated with some known absorption lines and a complete discontinuity at z_{abs} = 1.346.

4. 0237−233 (z_{em} = 2.223)

Absorption by Lyβ (2706 Å) is detected at the redshift of the intervening absorber at z_{abs} = 1.636. The corresponding Lyα absorption is in the low-sensitivity region of the long-wavelength detector and, hence, cannot be positively identified. Many metal-line absorption systems in the redshift range 2.2–1.36 have been observed in this quasar (Junkkarinen, Hewitt, & Burbidge 1991). The slope seen in the 2100–3100 Å continuum can be influenced by the Lyman absorption lines associated with the observed metal-line systems. The S/N in the spectrum is insufficient to detect a Lyman edge with any significance at the quasar emission redshift. A fit to the Lyman edge corresponding to the absorption system at 1.632 is shown in Figure 2.

5. 0302−223 (z_{em} = 1.400)

The Lyman edge in this quasar lies close to the joining between the LW and the SW cameras. The spectra were taken within 24 hr of each other, and the data show no evidence of error. Hence, the discontinuity in this spectra is not an artifact of joining the LW and SW spectra. In addition, the discontinuity lies at $\approx$2150 Å rather than lying exactly at the cutoff (2000 Å) between the cameras, which is an indication that the discontinuity is unlikely to be due to the fact that it lies close to the link between the LW and the SW cameras. Petitjean & Bergeron (1990) have observed strong Mg II absorption at z_{abs} = 1.01. The absorption features at $\approx$2400 and 2450 Å seem to indicate either a curved continuum shape or an emission-like feature. The overall spectrum shows no such features.

6. 0405−123 (z_{em} = 0.534)

This object (shown in full in Fig. 1*a*) is one of the strongest candidates for a partial discontinuity as predicted by accretion disk theory, being a partial discontinuity at the objects redshift, with good signal-to-noise ratio. The feature seen at 1485 Å is most probably a part of the 1500 Å artifact seen by Crenshaw et al. (1989). The absorption edge is not velocity broadened. Optical polarization observations by Antonucci (1992) show no polarization.

7. 0414−061 (z_{em} = 0.781)

This object has a strong feature at $\approx$1750 Å which could possibly be associated with N III] λ991.

8. 0454+039 (z_{em} = 1.345)

SW spectra are not available for this quasar, hence it is difficult to know exactly the nature of the discontinuity. Two metal absorption systems (z_{abs} = 0.859 and 1.153) have been detected (Petitjean & Bergeron 1990; Weymann et al. 1979). The system at z_{abs} = 1.153 can be associated with the decline in the flux observed by us. No significant discontinuity is observed at the quasar redshift.

9. 0537−441 (z_{em} = 0.894)

This object is known to vary. Since there are no simultaneous observations in both the cameras to help us normalize the variability, we have only used the SW region in the analysis. Since the significance of the Lyman edge discontinuity is low this object is included in Figure 3 as a "possible edge detection" and not in the analysis. There are no known absorption-line systems affecting the continuum and the slopes on either sides of the Lyman limit differ. 0537−441 is a weak candidate for a discontinuity caused by an accretion disk.

10. 0743−673 (z_{em} = 1.512)

The Lyman edge is redshifted to lie close to the cutoff of the LW camera in 0743−673. The fact that there are no SW spectra, as well as the low signal-to-noise ratio around 2100 Å, makes it difficult to evaluate the significance of the discontinuity. Even though the significance of the Lyman edge discontinuity is low this object is included in group 4 and not in group 1 because there are no known absorption-line systems affecting the continuum and the slopes on either sides of the Lyman limit differ. 0743−673 is a weak candidate for a discontinuity at the Lyman edge due to accretion disk, specially since the continuum tends to zero flux toward shorter wavelengths.

11. 0935+417 (z_{em} = 1.980)

This object contains a strong absorption feature at 2880 Å and a weaker absorption feature at 2570 Å, which may both be Lyman forest lines. The feature at 2880 Å may be Lyα absorption corresponding to the C IV absorption observed at z_{abs} = 1.372 by Bechtold et al. (1984). Lyman absorption features have not been included in the fitting procedure and hence, the emission-like feature just above 912 Å seems real.

12. 0955+326 (z_{em} = 0.533)

The significance of a discontinuity is low because the spectrum is dominated by artifacts. Hence this object is removed from the analysis and is included in Figure 3. Metal absorption lines have been observed at z_{abs} = 0.513 (Boksenberg & Sargent 1978), so that any discontinuity is unlikely to be associated with an accretion disk.

13. 1011+250 (z_{em} = 1.631)

The fit to the region shortward of the Lyman edge is not very appealing because of the large uncertainties in the flux. Possible absorption features are detected at 2800, 2580, and 2530 Å.

14. 1136−135 (z_{em} = 0.557)

The significance of a discontinuity is low because the spectrum is dominated by artifacts. Hence this objected is removed from the analysis and is included in Figure 3. There are no known absorption-line systems affecting the continuum. 1136−135 is a weak candidate for a discontinuity caused by an accretion disk.

15. 1225+317 (z_{em} = 2.219)

This object is known to have complex intervening absorption features in the optical (see Table 3 for references). In the *IUE* spectrum, many absorption features are seen below the Lyα emission line, which are presumably Lyα forest absorption features. Because of the absorption features the continuum in these fits is lower than the true continuum from the quasar.

16. 1241+176 (z_{em} = 1.273)

The continuum fit to the extrinsic Lyman discontinuity at z_{abs} = 0.567 for this object is problematical because of the low signal-to-noise ratio and the complex *IUE* artifacts around 1500 Å. The discontinuity at the quasar emission may not be real, as there are no simultaneous SW and LW spectra and the Lyman edge (2072 Å) lies close to the cutoff between the *IUE* cameras. This object is included in Figure 3 as "possible Lyman edge detection."

17. 1247+267 (z_{em} = 2.038)

This spectrum (shown in full in Fig. 1*c*) contains strong absorption features of the Lyα forest. The Lyα absorption features at 2697 Å (z_{abs} = 1.218) and 2920 Å (z_{abs} = 1.4063) from known absorption-line systems (see references in Table 3) influence the fitting procedure. Hence the fit to the Lyman edge is inconclusive for z = 2.038.

18. 1317+277 (z_{em} = 1.022)

This spectrum appears to contain rich Lyα absorption below the Lyα emission line in spite of its low redshift.

19. 1331+170 (z_{em} = 2.081)

The steep slope above 2400 Å in this spectrum is influenced by many Lyman absorption lines associated to the metal absorption systems (especially z_{abs} = 1.327) seen in the optical by other investigators (see Table 3 for references). We observe a complete discontinuity at z_{abs} = 1.807. The significance of the discontinuity is not very high because of the large change in slope for the fits on either side of the Lyman edge.

20. 1338+416 (z_{em} = 1.219)

This object has a strong partial discontinuity which is slightly blueshifted from the quasar redshift. Only a 300 Å region in the quasar rest frame was used in the fitting procedure because the spectrum had some nonstatistical noise.

21. 1354+195 (z_{em} = 0.720)

The spectrum of this object is contaminated by a cosmic ray hit at ≈1380 Å which was not included in the fit.

22. 1522+101 (z_{em} = 1.321)

The SW and LW spectra are not observed simultaneously in this object and the Lyman edge is in the region where the spectra of the two cameras join. Therefore, the intrinsic Lyman edge detected is not significant and in Figure 2 only the power-law fit across the Lyman edge is shown. There is evidence of a $z_{abs} < z_{em}$ system with no associated metal absorption lines observed in the literature.

23. 1538+477 (z_{em} = 0.770)

This object shows what may be a very deep extended partial discontinuity at the redshift of the object or may be a changing continuum. Since there are no detected or reported narrow absorption lines at the object redshift, this discontinuity is a candidate for the type of discontinuity due to an accretion disk.

24. 1630+377 (z_{em} = 1.471)

The SW and LW spectra are not observed simultaneously. Therefore, the intrinsic Lyman edge detected is not significant, and in Figure 2 only the power-law fit across the Lyman edge is shown.

25. $1634+706$ ($z_{em} = 1.334$)

This object appears to have a complex Lyα forest. Complete absorption at $z_{abs} = 0.984$ and partial absorption at $z_{abs} = 1.047$ have been detected, which correspond to the $z_{abs} = 0.993$ and 1.046 Mg II absorption systems observed by Bechtold et al. (1984). Further possible partial absorption is detected at $z = 1.334$, but the discontinuity can easily be due to the Lyβ absorption lines of the two absorption-line systems mentioned.

26. $1641+399$ ($z_{em} = 0.595$)

The spectrum is affected by the broad artifact at 1500 Å, but still has a significant partial discontinuity. Ellingson, Green, & Yee (1991) have observed a galaxy associated with this quasar at $z = 0.594$. The partial discontinuity in this object may be due to this companion galaxy.

27. $1715+535$ ($z_{em} = 1.920$)

This object has two observed metal absorption-line systems (Sargent, Boksenberg, & Steidel 1988). Lyα absorption lines associated with these absorption-line systems are probably affecting the continuum at wavelengths shorter than Lyα.

28. $1718+481$ ($z_{em} = 1.084$)

This object contains a partial discontinuity at a lower redshift than that of the object. The discontinuity is recovering with a slope of $\approx \nu^{-3}$.

29. $2302+029$ ($z_{em} = 1.044$)

The Lyman edge close to the region where the spectra of the SW and LW cameras join. Also the SW and LW spectra are not observed simultaneously. Therefore, the intrinsic Lyman edge detected is not significant, and in Figure 2 only the power-law fit across the Lyman edge is shown.

30. $2308+098$ ($z_{em} = 0.432$)

This spectrum is artifact-dominated, and only 48 data points are available below the Lyman edge for the fitting procedure. These factors reduce the significance of the discontinuity detected.

REFERENCES

Angel, J. R. P., & Stockman, H. S. 1980, ARA&A, 18, 321
Antonucci, R. R. J. 1987, in Supermassive Black Holes, ed. M. Kaftos (Cambridge Univ. Press), 26
———. 1992, in Proc. 2d Ann. October Astrophysics Conf. Testing the AGN Paradigm, ed. S. S. Holt, S. G. Neff, & C. M. Urry (New York: AIP), 486
Antonucci, R. R. J., Kinney, A. L., & Ford, H. C. 1989, ApJ, 342, 64
Baldwin, J., & Smith, M. G. 1983, MNRAS, 204, 331
Bechtold, J., Green, R. F., Weymann, R. J., Schmidt, J., Estabrook, F. B., Sherman, R. D., Wahlquist, H. D., & Heckman, T. M. 1984, ApJ, 281, 76
Bechtold, J., Green, R. F., & York, D. G. 1987, ApJ, 312, 50
Begelman, M. C. 1985, in Astrophysics of Active Galactic Nuclei and Quasi-Stellar Objects, ed. J. Miller (Mill Valley, CA: University Science Books), 411
Bergeron, J. 1986, A&A, 155, 18
Bergeron, J., & Boisse, P. 1986, A&A, 168, 6
Bergeron, J., & Kunth, D. 1983, MNRAS, 205, 1053
Blades, J. C., Hunstead, R. W., Murdoch, H. S., & Pettini, M. 1983, MNRAS, 200, 1091
Blades. J. C., et al. 1985, ApJ, 288, 580
Boisse, P., & Bergeron, J. 1985, A&A, 145, 59
Boksenberg, A., Carswell, R. F., & Sargent, W. L. W. 1979, ApJ, 227, 370
Boksenberg, A., & Sargent, W. L. W. 1978, ApJ, 220, 42
Boroson, T., Sargent, W. L. W., Young, P., Boksenberg, A., & Carswell, R. F. 1978, ApJ, 220, 772
Bergman, J. N., Glassgold, A. E., & Huggins, P. J. 1981, ApJ, 249, 13
Burstein, D., & Heiles, C. 1982, AJ, 87, 1165
Carswell, R. F., & Ferland, G. 1988, MNRAS, 235, 1121
Carswell, R. F., Whelan, J. A. J., Smith, M. G., Boksenberg, A., & Tytler, D. 1982, MNRAS, 198, 91
Caulet, A. 1989, ApJ, 340, 90
Czerny, B., & Pojmanski, G. 1990, MNRAS, 245, 1
Czerny, B., & Zbyszewska, M. 1991, MNRAS, 249, 643
Collin-Souffrin, S., & Dumont, A. M. 1990, A&A, 229, 313
Crenshaw, M. D., Bruegman, O. W., & Norman, D. J. 1990, PASP, 102, 463
Ellingson, E., Green, R. F., & Yee, H. K. C. 1991, ApJ, 378, 476
Eracleous, M., & Halpren, J. 1992a, in Proc. 2d Ann. October Astrophysics Conf., Testing the AGN Paradigm, ed. S. S. Holt, S. G. Neff, & C. M. Urry (New York: AIP), 216
———. 1992b, in Proc. Ann. October Astrophysics Conf., Testing the Paradigm, ed. S. S. Holt, S. G. Neff, & G. M. Urry (New York: AIP), 220
Foltz, R., Weymann, R. J., Peterson, B. M., Sun, L., Malkan, M. A., & Chaffee, H. 1986, ApJ, 307, 504
Green, R., et al. 1980, ApJ, 239, 483
Hewitt, P., & Burbidge, G. 1987, ApJS, 63, 1
Junkkarinen, V., Hewitt, P., & Burbidge, G. 1991, ApJS, 77, 203
Kinney, A. L., Bohlin, R. C., Blades, J. C., & York, D. G. 1991a, ApJS, 75, 645
Kinney, A. L., Bohlin, R. C., & Neill, J. D. 1991b, PASP, 103, 694
Kolykhalov, P. I., & Sunyaev, R. A. 1984, Adv. Space Res., 3, 249
Kwan, J., & Krolik, J. H. 1981, ApJ, 250, 478
Lanzetta, K. M. 1988, ApJ, 332, 96
Lanzetta, K. M., Turnshek, D. A., & Wolfe, A. M. 1987, ApJ, 322, 739
Laor, A., & Netzer, H. 1989, MNRAS, 238, 879
———. 1992, in Proc. 2d Ann. October Astrophysics Conf., Testing the AGN Paradigm, ed S. S. Holt, S. G. Neff, & C. M. Urry (New York: AIP), 155
Laor, A., Netzer, H., & Piran. 1990, MNRAS, 242, 560
Lynden-Bell, D. 1969, Nature, 223, 690
MacAlpine, G. M., & Feldman, F. R. 1982, ApJ, 261, 412
Malkan, M. A. 1983, ApJ, 268, 582
Moore, R. L., & Stockman, H. S. 1981, ApJ, 234, 60
Netzer, H. 1992, in Proc. 2d Ann. October Astrophysics Conf., Testing the Paradigm, ed. S. S. Holt, S. G. Neff, & G. M. Urry (New York: AIP), 146
O'Brien, P., et al. 1988, MNRAS, 233, 801
Petitjean, P., & Bergeron, J. 1990, A&A, 231, 309
Salpeter, E. E. 1964, ApJ, 140, 796
Sargent, W. L. W., Boksenberg, A., & Steidel, C. C. 1988, ApJS, 68, 539
Sargent, W. L. W., Young, P., Boksenberg, A., & Tytler, D. 1980, ApJS,
Shields, G. 1978, Nature, 272, 706
Smith, M. G., Carswell, R. F., Whelan, J. A. J., Wilkes, B. J., Boksenberg, A., Clowes, R. G., Savage, A., Cannon, R. D., & Wall, J. V. 1981, MNRAS, 195, 437
Snijders, M. A. J., Pettini, M., & Boksenberg, A. 1981, ApJ, 245, 386
Sofia, U. J., Bruhweiler, F. C., & Kafatos, M. 1989, A Decade of UV Astronomy with the *IUE* Satellite, ESA SP-281, 269, ed. E. J. Rolfe (Noordwijk: ESA ESTEC)
Steidel, C. C., & Sargent, W. L. W., 1987, ApJ, 313, 171
Sun, W. H., & Malkan, M. A. 1989a, in Active Galactic Nuclei, ed. D. E. Osterbrock & J. S. Miller (Dordrecht: Reidel), 262
———. 1989b, ApJ, 346, 68
Tytler, D., Boksenberg, A., Sargent, W. L. W., Young, P., & Kunth, D. 1987, ApJS, 64, 667
Veron-Cetty, M. P., & Veron, P. 1987, ESO Scientific Rep., No. 5, p. 1
Weymann, R. J., Williams, R. E., Peterson, B. M., & Turnshek, D. A. 1979, ApJ, 234, 33
Young, P., Sargent, W. L. W., & Boksenberg, A. 1982, ApJ, 252, 10
———. 1982b, ApJS, 48, 455
Zel'dovich, Y. B., & Novikov, I. B. 1964, Dokl. Acad. Nauk SSSR, 158, 811